





Article

Novel Substrates for Kinases Involved in the Biosynthesis of Inositol Pyrophosphates and Their Enhancement of ATPase Activity of a Kinase

Raja Mohanrao ¹, Ruth Manorama ², Shubhra Ganguli ^{2,3}, Mithun C. Madhusudhanan ¹, Rashna Bhandari ^{2,*}
and Kana M. Sureshan ^{1,*}

¹ School of Chemistry, Indian Institute of Science Education and Research Thiruvananthapuram, Kerala 695551, India; rajamohanrao1@gmail.com (R.M.); mithun716@iisertvm.ac.in (M.C.M.)

² Laboratory of Cell Signalling, Centre for DNA Fingerprinting and Diagnostics, Hyderabad 500039, India; manorama@cdfd.org.in (R.M.); shubhraganguli@cdfd.org.in (S.G.)

³ Manipal Academy of Higher Education, Manipal 576104, India

* Correspondence: rashna@cdfd.org.in (R.B.); kms@iisertvm.ac.in (K.M.S.)

Abstract: IP6K and PPIP5K are two kinases involved in the synthesis of inositol pyrophosphates. Synthetic analogs or mimics are necessary to understand the substrate specificity of these enzymes and to find molecules that can alter inositol pyrophosphate synthesis. In this context, we synthesized four *scyllo*-inositol polyphosphates—*scyllo*-IP₅, *scyllo*-IP₆, *scyllo*-IP₇ and Bz-*scyllo*-IP₅—from *myo*-inositol and studied their activity as substrates for mouse IP6K1 and the catalytic domain of VIP1, the budding yeast variant of PPIP5K. We incubated these *scyllo*-inositol polyphosphates with these kinases and ATP as the phosphate donor. We tracked enzyme activity by measuring the amount of radiolabeled *scyllo*-inositol pyrophosphate product formed and the amount of ATP consumed. All *scyllo*-inositol polyphosphates are substrates for both the kinases but they are weaker than the corresponding *myo*-inositol phosphate. Our study reveals the importance of axial-hydroxyl/phosphate for IP6K1 substrate recognition. We found that all these derivatives enhance the ATPase activity of VIP1. We found very weak ligand-induced ATPase activity for IP6K1. Benzoyl-*scyllo*-IP₅ was the most potent ligand to induce IP6K1 ATPase activity despite being a weak substrate. This compound could have potential as a competitive inhibitor.

Keywords: kinase; inositol pyrophosphate; IP6K1; VIP1 KD; ATPase



Citation: Mohanrao, R.; Manorama, R.; Ganguli, S.; Madhusudhanan, M.C.; Bhandari, R.; Sureshan, K.M. Novel Substrates for Kinases Involved in the Biosynthesis of Inositol Pyrophosphates and Their Enhancement of ATPase Activity of a Kinase. *Molecules* **2021**, *26*, 3601. <https://doi.org/10.3390/molecules26123601>

Academic Editors: Brullo Chiara, Marie Migaud and Gerd Wagner

Received: 6 May 2021

Accepted: 7 June 2021

Published: 11 June 2021

Publisher's Note: MDPI stays neutral with regard to jurisdictional claims in published maps and institutional affiliations.



Copyright: © 2021 by the authors. Licensee MDPI, Basel, Switzerland. This article is an open access article distributed under the terms and conditions of the Creative Commons Attribution (CC BY) license (<https://creativecommons.org/licenses/by/4.0/>).

1. Introduction

Phosphoinositols play a variety of roles in cellular signaling [1,2]. Diphospho-inositol polyphosphates (PPIPns) are a class of highly phosphorylated *myo*-inositol derivatives that have one or two pyrophosphate moieties and occur only in eukaryotes [3–5]. PPIPns present in mammals include 5-PP-IP₄, 5-PP-IP₅, 1-PP-IP₅ and 1,5-[PP]₂-IP₄, and their cellular levels are regulated by (i) IP6Ks, kinases which pyrophosphorylate the 5-position of *myo*-inositol, (ii) PPIP5Ks, kinases which pyrophosphorylate the 1-position and (iii) DIPPs, phosphatases which dephosphorylate the pyrophosphate to phosphate (Figure 1A) [6–8]. PPIPns play vital roles in apoptosis, cellular signaling, vesicular trafficking, metabolic homeostasis, cytoskeletal dynamics, exocytosis, insulin signaling, DNA damage repair, telomere maintenance, stress response, etc. [4,9–24]. Clear mechanisms of their wide-ranging functions are yet to be ascertained [23,25–27]. For biochemical and genetic exploration to unravel the structure-activity relationships (SAR) and mechanism of their actions, it is necessary to synthesize these molecules and their analogs [2,22,28–30]. Recently, Jessen et al. reported elegant approaches to synthesize various PPIPn analogs [31–33]. These analogs served as tools to unravel various biological roles played by inositol pyrophosphates [34]. Potter et al. [35] and Fiedler et al. [29,36,37] independently synthesized PPIPn analogs

having non-hydrolyzable pyrophosphate surrogates and established, through biochemical assays, that this modification does not prevent target recognition and action of metabolizing enzymes. Both of these studies have also established that the recognizing enzymes can tolerate 2-O-substitution with a hydrophobic group. An extension of this study not only validated the previously reported [38] ligand induced ATPase activity of one of the kinases, PPIP5K2, but also unraveled the mechanism for the same [39]. Here we report the syntheses and biochemical studies of four novel substrate analogs of kinases involved in PPIPn biosynthesis, and ATPase activities of both these kinases.

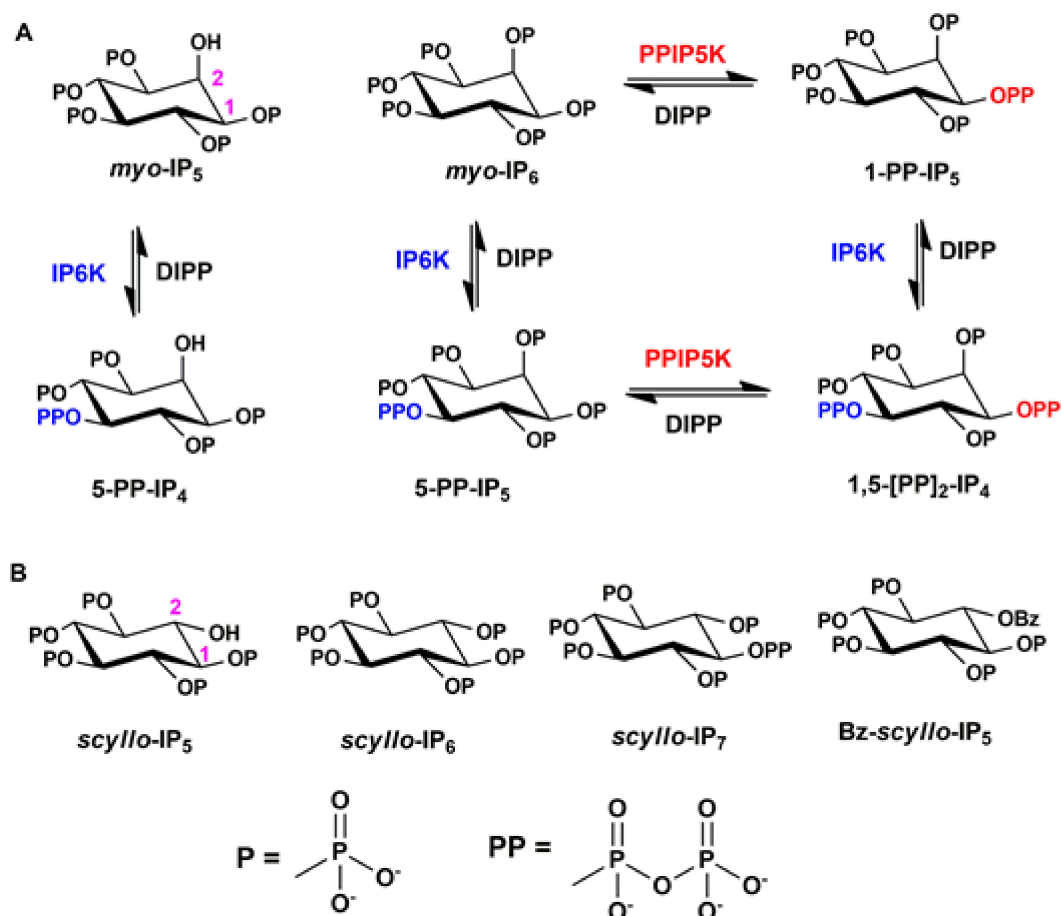


Figure 1. (A) Biosynthesis of inositol pyrophosphates in mammalian cells. (B) Proposed ligands to probe kinase activity.

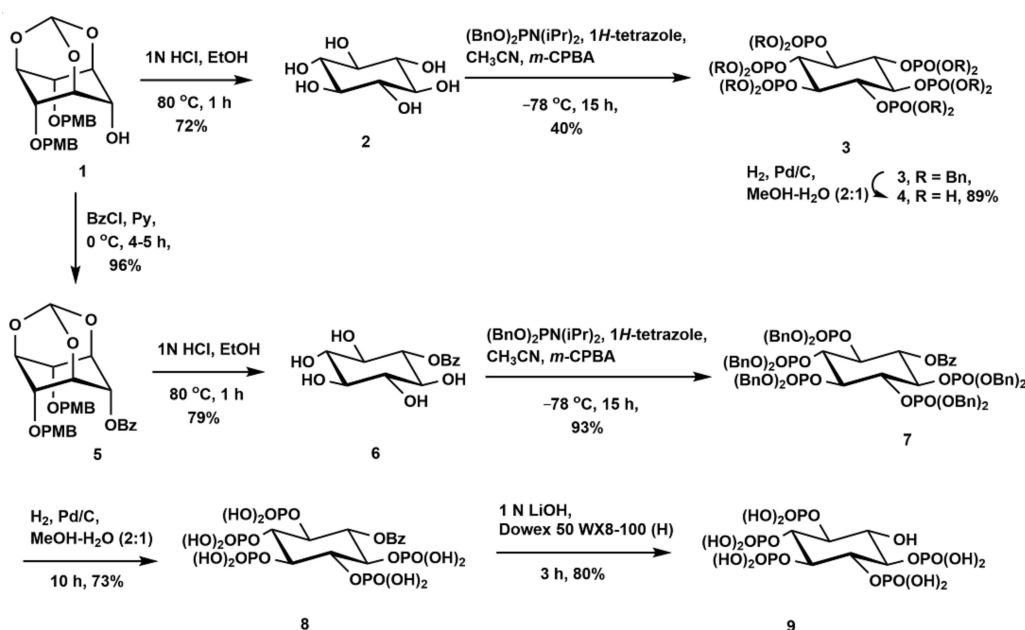
As mentioned earlier, IP6Ks and PPIP5Ks are involved in the biosynthesis of PPIPns. IP_5 , IP_6 and 1-PP-IP_5 are the natural substrates for IP6Ks and get phosphorylated to 5-PP-IP_4 , 5-PP-IP_5 and $\text{1,5-[PP]}_2\text{-IP}_4$, respectively (Figure 1A). Similarly, IP_6 and 5-PP-IP_5 are the natural substrates for PPIP5Ks and get phosphorylated to 1-PP-IP_5 and $\text{1,5-[PP]}_2\text{-IP}_4$, respectively (Figure 1A) [40–43]. There is great interest in understanding the mechanism, function and substrate-specificity of these enzymes using various analogs as synthetic tools [30,35,36,39,44]. An important strategy to make analogs of IPns is to alter the inositol core. We chose *scyllo*-inositol, the C2-epimer of *myo*-inositol as the central core to synthesize PPIPn analogs. *Scyllo*-inositol phosphates constitute the second naturally abundant inositol phosphates [45–47] and many *scyllo*-inositol phosphates have been found in living organisms and in the environment [48,49]. Utilizing these *scyllo*-inositol phosphates as substrates for the PPIPn synthesizing kinases, would provide valuable information regarding enzyme function. In this context, we planned to synthesize *scyllo-IP*₅, *scyllo-IP*₆ and *scyllo-IP*₇ (Figure 1B) to test them as substrates for Vip1 (budding yeast *S. cerevisiae* ortholog of PPIP5K) and mouse IP6K1. While the first two are mimics of IP_5 and IP_6

respectively, *scyllo*-IP₇ is a mimic of both 1-PP-IP₅ and 5-PP-IP₅. We also planned to synthesize Bz-*scyllo*-IP₅, as 2-*O*-benzyl/2-*O*-benzoyl substituted ligands are known to activate PPIP5K2 [39].

2. Results and Discussion

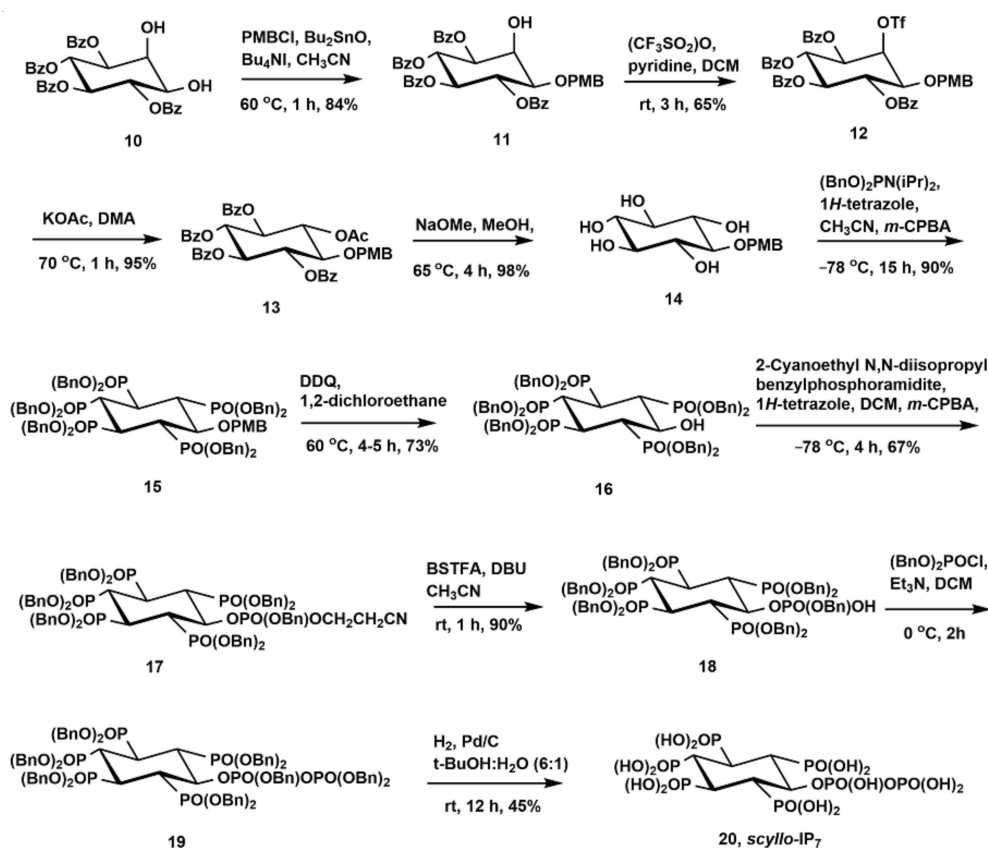
2.1. Synthesis of *Scyllo*-Inositol Phosphates

Scyllo-inositol derivative **1** was synthesized from *myo*-inositol in four steps by following the reported procedure [45]. Acidic hydrolysis of **1** with 1 N HCl in ethanol yielded *scyllo*-inositol (**2**), which, on phosphitylation with *N,N*-dibenzyl diisopropylphosphoramidite in the presence of 1*H*-tetrazole followed by oxidation with *m*-CPBA at -78 °C, gave hexaphosphorylated *scyllo*-inositol derivative **3** (Scheme 1). Hydrogenolysis of **3** yielded *scyllo*-IP₆ (**4**). Benzoylation of **1** followed by acidic hydrolysis of the ester **5** gave benzoyl-*scyllo*-inositol (**6**). Phosphorylation of **6** resulted in the fully protected *scyllo*-inositol pentakisphosphate (**7**), which, on hydrogenolysis, yielded the benzoyl-*scyllo*-IP₅ (**8**). Compound **8** on treatment with 1 N LiOH gave *scyllo*-IP₅ (**9**), which was purified by passing through Dowex H⁺ resin.



Scheme 1. Synthesis of *scyllo*-IP₆ (**4**), Bz-*scyllo*-IP₅ (**8**) and *scyllo*-IP₅ (**9**).

Next, we turned our attention to synthesize *scyllo*-IP₇ (Scheme 2). Attempts to remove the benzoyl group selectively from compound **7** failed. This prompted us to pursue another approach for the synthesis of *scyllo*-IP₇ (**20**) starting from *myo*-inositol derivative **10** [50]. Selective *O*-alkylation of the equatorial hydroxyl group using *p*-methoxybenzyl chloride gave compound **11**, which, on triflylation, gave the triflate **12**. Nucleophilic displacement of the triflate with acetate gave *scyllo*-inositol derivative **13**, which, on saponification, yielded the pentol **14**. Phosphitylation of pentol **14** followed by in situ oxidation resulted in the formation of fully protected pentakisphosphate **15**. Oxidative removal of the PMB group afforded compound **16**, whose structure was unambiguously confirmed by single crystal XRD analysis (see Figure 7 in Section 3.2.15., Crystal Data for **16**). Compound **16** was then phosphitylated with the unsymmetrical phosphoramidate, 2-cyanoethyl-*N,N*-diisopropyl benzylphosphoramidite (see Scheme 3 in Section 3.2.16.), followed by oxidation to get differently protected hexakisphosphate derivative **17**. Deprotection of the cyanoethyl group gave the phosphodiester **18**. Phosphorylation of **18** using dibenzylphosphoryl chloride [30,51] yielded fully protected *scyllo*-IP₇ derivative **19**, which was used without purification for hydrogenolysis to get the *scyllo*-IP₇ (**20**).

Scheme 2. Synthesis of *scyllo*-IP₇ (20).

2.2. Analysis of *Scyllo*-Inositol Phosphates as Substrates for IP6K and PPIP5K

We investigated the ability of these *scyllo*-inositol phosphates to act as substrates for mouse IP6K1 (UniProt entry Q6PD10) and *S. cerevisiae* VIP1 (UniProt entry Q06685) in comparison with *myo*-IP₅ and IP₆. All these substrate analogs were incubated with ATP and purified *N*-terminally 6xHis-tagged mouse IP6K1 or the kinase domain (amino acid residues 1–535) of *S. cerevisiae* VIP1 fused *N*-terminally to GST (VIP1-KD). The IP_n substrates and their PPIP_n products were resolved by polyacrylamide gel electrophoresis (PAGE) and detected by staining with toluidine blue dye (Section 3.3). Upon the incubation of *myo*-IP₅ or *myo*-IP₆ with IP6K1 or VIP1-KD, we detected one or more *myo*-PPIP_n products (Supplementary Figure S1). Our observations are in concordance with an earlier report demonstrating multiple PP-IP products arising from the action of these IP kinases on *myo*-IP₅ or *myo*-IP₆, many of which are uncharacterized [52]. All *scyllo*-IP_ns served as substrates for both IP6K1 and VIP1-KD (Supplementary Figure S1). PAGE analysis of PP-IPs is not suitable for the quantitative comparison of *scyllo*- vs. *myo*-IPs as substrates, owing to the variation in staining of different IP_ns by toluidine blue dye. Therefore, to quantify the PPIP_n products arising from *myo*- and *scyllo*-IP_n substrates, we resorted to the use of radiolabeled ATP. Equimolar quantities of the different IP_n substrates were incubated with either enzyme in the presence of [γ -³²P]ATP; the enzymatic reactions were quenched by adding perchloric acid and then neutralized with potassium carbonate and EDTA (Section 3.3). The products were separated by strong anion exchange HPLC, and 1 mL fractions were collected and counted using a liquid scintillation counter. The substrates and the corresponding chromatograms showing the peaks due to phosphorylated products are shown in Figure 2. Each HPLC peak represents the addition of a radiolabeled phosphate onto the IP_n substrate. Owing to the inability to use an ATP regeneration system along with radiolabeled ATP (see Section 3.3), in many cases, we observed fewer products by HPLC compared with PAGE analysis.

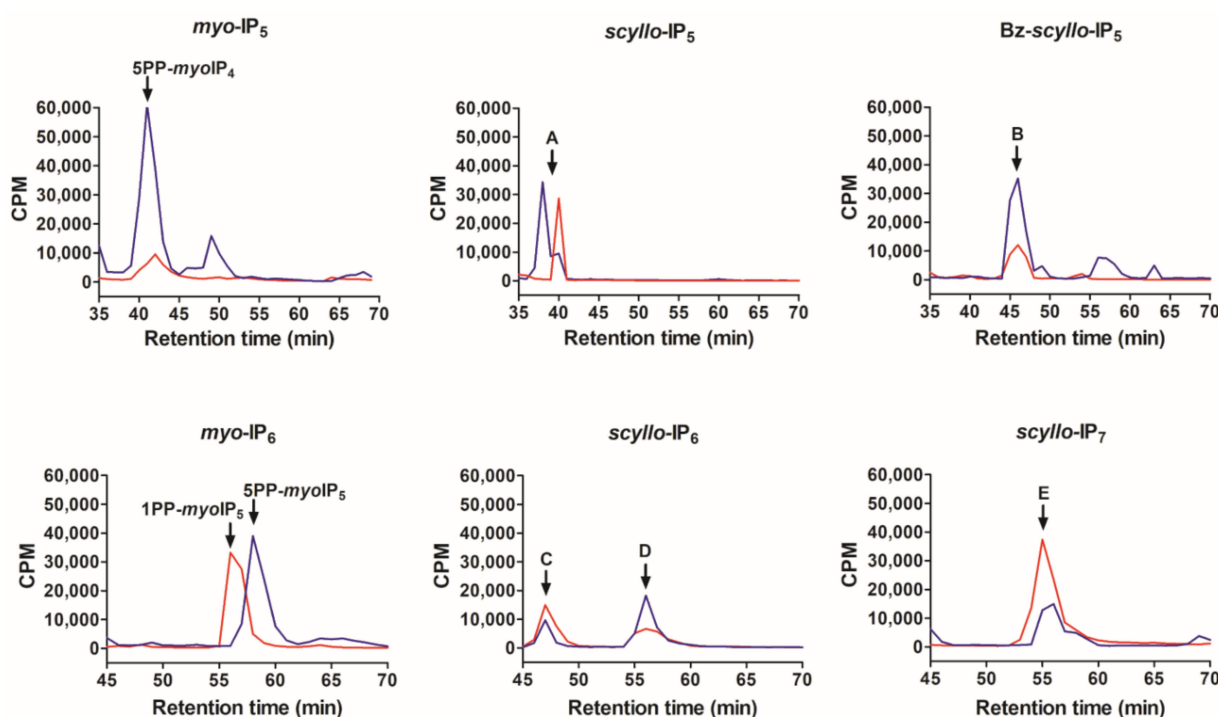


Figure 2. Chromatograms of the phosphorylated PIPn products (indicated by arrows) formed by the catalysis of IP6K1 (blue) and VIP1-KD (red) on various IPn substrates. The IPn substrate used in each case is indicated above the chromatogram. The reaction products were resolved by strong anion exchange HPLC as described in Section 3.3. Retention times for standard *myo*-IPs were marked using radiolabeled inositol phosphates extracted from budding yeast (Section 3.3 and Supplementary Figure S2B). The traces represent one of four independent experiments. The well-characterized products of *myo*-IP₅ and *myo*-IP₆ are indicated. The PPIPn products of *scyllo*-IPs are likely to be as follows: A. PP-*scyllo*-IP₄; B. PP-Bz-*scyllo*-IP₄; C. PP-*scyllo*-IP₅; D. [PP]₂-*scyllo*-IP₄/PPP-*scyllo*-IP₅; E. [PP]₂-*scyllo*-IP₄/PPP-*scyllo*-IP₅. The corresponding PPIPn products observed by PAGE analysis are similarly annotated in Figure S1. See Figure S2B,C for chromatograms of other *myo*-IPn and *myo*-PPIPn standards, and ATP, under the same conditions.

We have proposed probable structures for the *scyllo*-PPIPn products seen by gel electrophoresis and HPLC (see legends for Figure 2 and Supplementary Figure S1). Our proposed structures are based on the known catalytic properties of IP6K1 and VIP1 towards *myo*-inositol substrates. IP6K1 catalyzes the addition of a β -phosphate onto an α -phosphate, and a γ -phosphate onto a β -phosphate on C5 of *myo*-IP₅ and *myo*-IP₆ [19,53], whereas VIP1 acts to add a β -phosphate on C1 of *myo*-IP₆ and *myo*-IP₇ [13,17]. As all equatorial carbon atoms of *scyllo*-inositol are indistinguishable from each other, we propose that the same *scyllo*-PPIPn products arise by the action of both enzymes. Therefore, IP6K1 and VIP1 probably act on *scyllo*-IP₅, Bz-*scyllo*-IP₅ and *scyllo*-IP₆ to yield PP-*scyllo*-IP₄, PP-Bz-*scyllo*-IP₄ and PP-*scyllo*-IP₅ (i.e., *scyllo*-IP₇), respectively (peaks A, B and C in Figure 2). The product formed by the addition of two phosphates onto *scyllo*-IP₆ (peak D), and one phosphate onto *scyllo*-IP₇ (peak E), are likely to correspond to a *scyllo*-inositol with 8 phosphate groups. This could be [PP]₂-*scyllo*-IP₄ or PPP-*scyllo*-IP₅. The only unambiguous means of identifying the structures of any of the *scyllo*-PPIPn products is via NMR. However, it is not trivial to obtain sufficient quantities of purified, enzymatically synthesized PPIPn products required for such an analysis. The masses of the products we have proposed are based on the bands visualized by PAGE (separated by a single phosphate units), and the resolution of ³²P-labeled inositol phosphates by HPLC. Despite repeated attempts we were unable to detect enzymatically synthesized *scyllo*-PPIPn products by mass spectrometry—HPLC-purified radiolabeled products cannot be loaded onto a mass spectrometer due to radiation safety protocols, and contaminating substances from polyacrylamide gels interfered with our attempts to analyze gel-eluted *scyllo*-IPs. For the above reasons, the

proposed structures of the *scyllo*-PPIP_n products detected by PAGE and HPLC analysis are likely, but not certain.

Analysis of the conversion of the substrates to products indicates that all *scyllo*-IP_ns tested are substrates for IP6K1, but they are relatively poorer substrates than the corresponding *myo*-inositol phosphates (Figure 3A). For IP6K1, *myo*-IP₅ shows the best conversion rate and is approximately 1.5-fold the conversion rate of *myo*-IP₆. This is in agreement with the trend reported previously [53]. Interestingly, *scyllo*-IP₅ and *scyllo*-IP₆ are poor substrates for IP6K1 compared with their *myo*-counterparts. This suggests that an axial C2-hydroxyl/phosphate has an important role in active-site binding. This requirement was however partially offset by the presence of a benzoyl group on *scyllo*-IP₅. It has been shown that IP6K1 can act on 5PP-*myo*-IP₅ to generate a triphosphate containing species—5PPP-*myo*-IP₅ [19]. We observed that IP6K1 can also act on *scyllo*-IP₇ to generate a product (Figure 2, peak E), which possibly contains a triphosphate moiety.

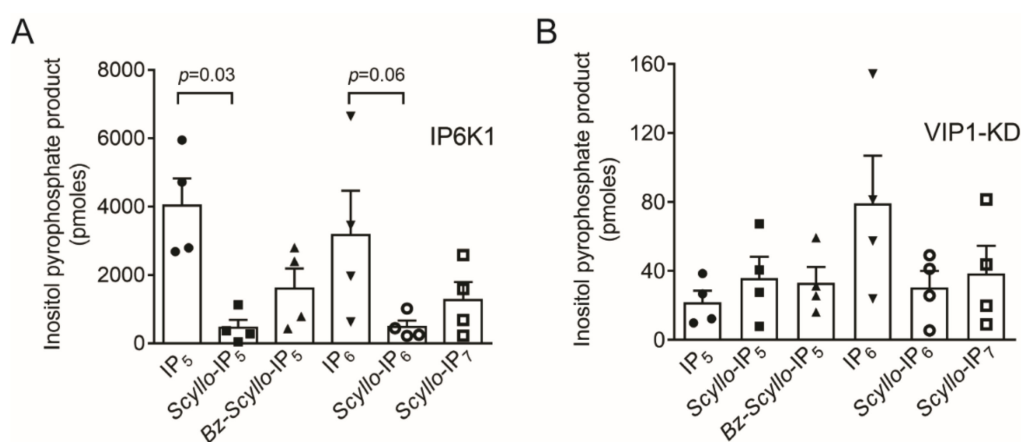


Figure 3. Extent of conversion of the substrates to products by (A) IP6K1 in presence of ATP (1 mM) and IP_n (200 μM). (B) VIP1-KD in presence of ATP (40 μM) and IP_n (100 μM). PPIP_n product formation was calculated as described in Section 3.3. The graphs show individual data points and mean ± SEM from four independent experiments. Data was analyzed using a two-tailed Mann–Whitney test to compare the PPIP_n product of *myo*-IP_n with its corresponding *scyllo*-derivative. *p* values are indicated where significant.

In contrast to IP6K1, all *scyllo*-IP_ns acted as moderate substrates for VIP1 (Figure 3B). *myo*-IP₅ is the poorest substrate of all those tested. This is in agreement with the fact that 1-PP-IP₄ has not been found in vivo and also with a previous report that *myo*-IP₅ is not a substrate for PPIP5Ks, mammalian orthologs of Vip1 [17]. *myo*-IP₆ is the best substrate; the approximately 3-fold difference between *myo*-IP₅ and *myo*-IP₆ phosphorylation by VIP1-KD suggests that the 2-phosphate is crucial for active site binding/effective phosphotransfer. All *scyllo*-IP_ns tested were weaker substrates for VIP1 compared with *myo*-IP₆, although the difference was not statistically significant. This suggests that the loss of the axial C2-phosphate can be partially compensated by an equatorial phosphate at that position. Interestingly, the presence of a benzoyl group on *scyllo*-IP₅ did not interfere with its ability to serve as a substrate for VIP1. It is to be noted that structurally similar 2-*O*-benzyl-*myo*-IP₅ was reported to be an inhibitor of PPIP5K but an activator of its ATPase activity [39].

In order to get further insights about the IP_n-kinase interactions, we conducted molecular docking with the kinases and *myo*-IP₆ and *scyllo*-IP₆ as ligands using CCDC GOLD suit (see Supplementary Materials and Supplementary Figure S3). Since exact structures for ScVIP1 and IP6K1 are not available, the molecular docking experiments were carried out at the active sites of analogous hPPIP5K2 and IP6KA kinase of *Entamoeba histolytica* (PDB code: 3T9C, 4O4F) [17,54]. With both the enzymes, *myo*-IP₆ showed better fitness score than *scyllo*-IP₆ and this is in agreement with the experimental observation of higher turnover for the *myo*-IP_ns. Furthermore, total number of attractive interactions between the enzyme and ligands was more for *myo*-IP₆ in both the cases. While *myo*-IP₆ had

21 interactions with IP6K, the *scyllo*-isomer had only 17 interactions. Similarly, PPIP5K2 kinase domain had 28 interactions with the *myo*-IP₆ and 26 interactions with the *scyllo*-IP₆. Interestingly, the axial C2 phosphate in *myo*-IP₆ shows seven interactions with the IP6K side-chains (K101, R119, S207, T106, R134), but the corresponding equatorial phosphate in *scyllo*-IP₆ shows four interactions (R119, K118, R134, T106). In the case of PPIP5K2, the axial phosphate at C2 position shows seven interactions (K329, R262, K248, R281, Y250) and equatorial phosphate makes five interactions (K329, K248, R262, R281) (Figure 4). This difference in number and strength of such interactions can influence the substrate binding and, thus, the kinase activity.

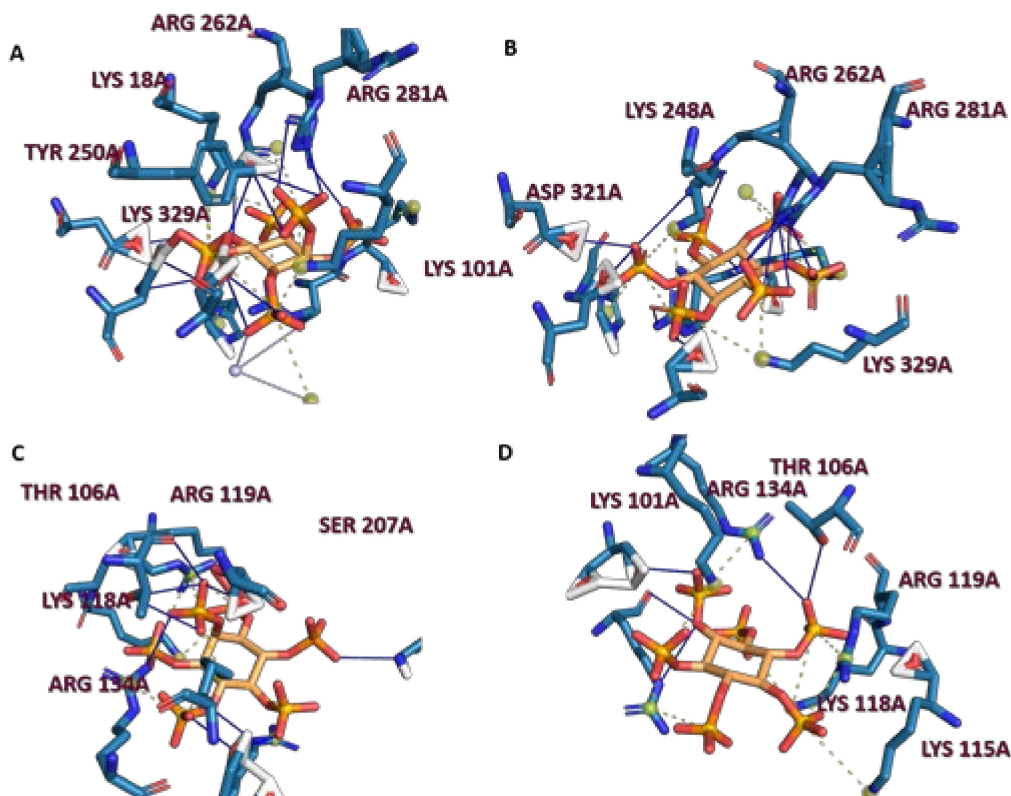


Figure 4. Molecular Docking results of *myo* and *scyllo*-IP₆ on PPIP5K2 and EhIP6KA (GOLDScore); (A) *myo*-IP₆ at the active site of PPIP5K2; (B) *scyllo*-IP₆ at the active site of PPIP5K2; (C) *myo*-IP₆ at the active site of EhIP6KA; (D) *scyllo*-IP₆ at the active site of EhIP6KA. All interactions were visualized using PLIP while further image processing was carried out using PyMOL [55].

The non-productive activation of PPIP5K2 by inositol phosphates leading to the hydrolysis of ATP to ADP (ATPase activity) has been reported [38]. Later, biochemical studies and mutagenesis studies, using several synthetic analogs, revealed the existence of a surface-exposed second binding site within the kinase domain of PPIP5K2, which acts as a capture site for the substrate, and that the natural substrate occupies this site only transiently before being delivered to the catalytic site [39]. The ATPase activity was found to be associated with ligand occupancy at the capture site. This study also found that 2-*O*-benzyl-*myo*-IP₅ interacts weakly with the catalytic site but binds better at the capture site of PPIP5K2, and consequently it is not a substrate of this kinase but a ligand that induces its ATPase activity [39]. We were curious to investigate the ability of *scyllo*-inositol phosphates to induce the ATPase activity of VIP1. A recent report describing a high-throughput assay for IP6K1 activity suggested that measuring ADP production from ATP is an easier alternative to HPLC-based measurement of 5-PP-IP₅ produced from IP₆ [56]. By extension, PPIP_n products of *scyllo*-IPs should also lead to concomitant ADP release from ATP, which can be used to measure kinase activity against these substrates. Furthermore,

many kinases are known to possess inherent ATPase activity [57–63], and PPIP5K2 shows substrate-stimulated ATP hydrolysis (38, 39). With these considerations, we studied ADP production by both kinases, IP6K1 and VIP1-KD. We ruled out the presence of any contaminating ATPase or phosphatase in the preparation of 6xHis-mIP6K1 or GST-VIP1-KD purified from the *E. coli* expression system (see Section 3.4 and Supplementary Figure S4).

We used the ADP-Glo™ kinase assay kit to monitor the conversion of ATP to ADP by IP6K1 and VIP1-KD in the presence of their IP substrates (Section 3.4) [56]. ADP-Glo™ kinase assay is a luminescence detection assay method to measure the percentage of ATP that is converted to ADP during a kinase reaction. VIP1-KD showed considerable basal activity, converting close to 40% of the ATP supplied during the reaction to ADP (Figure 5A), which is in agreement with its known inherent ATPase activity [38]. In contrast to the stimulation of non-productive ATPase activity by IP₅ and IP₆ reported in the case of PPIP5K2 [38,39], in our hands, both IP₅ and IP₆ showed only negligible ATPase activation of VIP1 over the basal level (Figure 6A). This may be due to differences in the behavior of VIP1 and PPIP5K2. It may also be a reflection of the significantly lower levels of ATP used in our assay—at high concentrations of ATP (5–10 mM), the presence of IP₅ and IP₆ leads to a 2- to 4-fold elevation in the release of Pi from ATP by PPIP5K2 (38). Under physiological ATP concentrations, IP₅ or IP₆ may stimulate ATPase activity of the VIP1-KD; substrate-independent ATPase activity of VIP1-KD may also increase at physiological [ATP]. The 4–6% of ATP consumed in the presence of IP₆ (Figure 6A) is sufficient for the conversion of approximately 2% of IP₆ to 1-PP-IP₅, in agreement with the extent of product formation shown in Figure 3B. All the *scyllo*-IPns tested showed up to two-fold enhancement in ATPase activity of VIP1 (Figure 5A). Interestingly, *scyllo*-IP₅ and *scyllo*-IP₆ enhance ATPase activity four times more than their corresponding *myo*-IPns (Figure 6A). This property of *scyllo*-IP₅ and *scyllo*-IP₆ to induce non-productive ATPase activity while being moderate substrates, suggests that these ligands may bind better at the capture site than the catalytic site of VIP1. Bz-*scyllo*-IP₅ and *scyllo*-IP₇ are also potent inducers of VIP1 ATPase activity; while the ATPase activity of the former is in agreement with the previously reported effect of 2-*O*-benzyl substituted *myo*-IP₅ enhancing non-productive ATPase activity of PPIP5K2 [39], in case of the latter, the absence of an axial-phosphate group may weaken its interaction with the active site and thus increase its residence time at the capture site, stimulating futile ATPase activity.

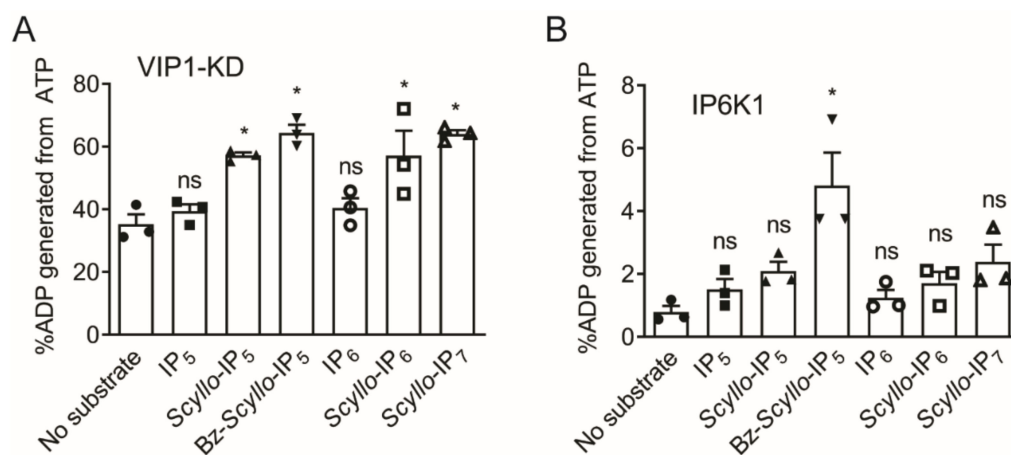


Figure 5. The effects of the *myo*- and *scyllo*-inositol phosphates upon ATPase activity of (A) VIP1-KD in presence of ATP (40 μ M) and IPn (100 μ M). (B) IP6K1 in presence of ATP (1 mM) and IPn (200 μ M). The graphs show individual data points and mean \pm SEM from three independent experiments. Data was analyzed using one-way ANOVA to compare each condition with ATPase activity in the absence of substrate. * $p \leq 0.05$; ns, not significant, $p > 0.05$.

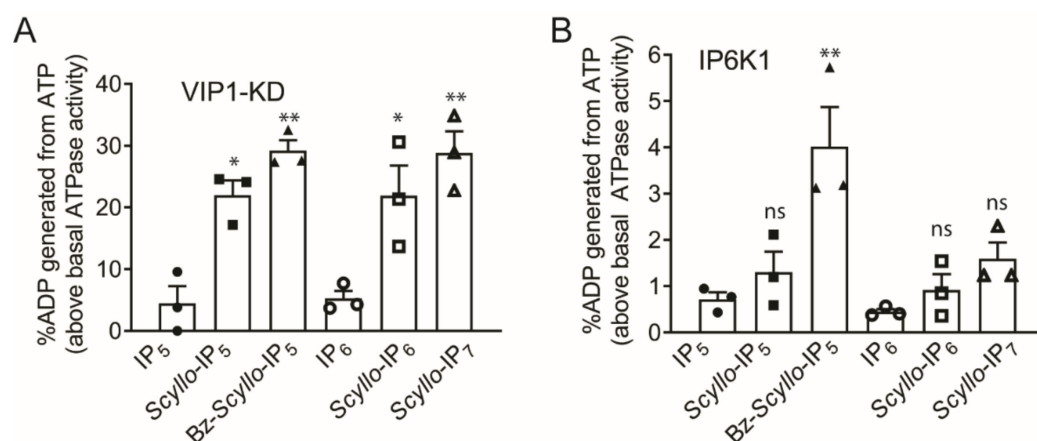


Figure 6. Percentage of ADP generated in the kinase reactions for (A) VIP1-KD and (B) IP6K1, after subtraction of basal ADP generated in the absence of substrate, for the data shown in Figure 5. The graphs show individual data points and mean \pm SEM from three independent experiments. Data was analyzed using one-way ANOVA to compare ATPase activity in the presence of each *scyllo*-IP_n with ATPase activity in the presence of either *myo*-IP₅ or *myo*-IP₆ (which were not significantly different from each other). ** $p \leq 0.01$; * $p \leq 0.05$; ns, not significant, $p > 0.05$.

IP6K1 showed a very low basal activity, suggesting that it is not an inherent ATPase (Figure 5B). The *myo*- and *scyllo*-inositol phosphates increased ADP production marginally (Figure 6B), in keeping with the transfer of the gamma phosphate from ATP to generate the corresponding inositol pyrophosphate (Figure 3A). An intriguing exception to this was Bz-*scyllo*-IP₅, which yielded a low amount of inositol pyrophosphate product, but significantly stimulated ATPase activity in IP6K1. Further studies will be required to establish non-productive ATPase activity in IP6K1.

In conclusion, we synthesized a series of *scyllo*-inositol phosphates as substrates for the two kinases involved in diphosphoinositol polyphosphate synthesis. This study revealed the tolerance of these enzymes for the *myo*- to *scyllo*- isomers. The relative potentials of these compounds as substrates in comparison with natural *myo*-inositol based substrates gave details and structural factors influencing binding of substrate to the enzymes. This study established that the absence of an axial hydroxyl/phosphate at the C2 position of an inositol phosphate reduces its potential as a substrate for IP6K1. In contrast, VIP1 appeared to accommodate the absence of an axial-2-phosphate more easily compared with IP6K1. All the *scyllo*-inositol derivatives tested are efficient in enhancing the ATPase activity of VIP1, which may be due to the preference of these compounds for the capture site on VIP1. Design of novel inhibitors based on these SAR studies and studies to identify the structures and biological effects of the products of these unnatural substrates are underway.

3. Materials and Methods

3.1. General

All chemicals and solvents were purchased from commercial suppliers and used directly. Solvents were dried using standard laboratory procedures and stored under anhydrous conditions. Reactions were monitored by thin layer chromatography (TLC) using Merck pre-coated silica plates (60 F254) (Darmstadt, Germany). TLC plates were visualized under ultraviolet light at 254 nm and also by charring using cerium ammonium molybdate solution (235 mL of distilled water, 12 g of ammonium molybdate, 0.5 g of cerium sulfate and 15 mL of concentrated sulphuric acid). Column chromatography was performed on silica gel (200–400 mesh). ¹H, ¹⁹F, ¹³C and ³¹P-NMR spectra were recorded using 500, 470, 125 and 202.4 MHz NMR spectrometers (Bruker, Mannheim, Germany), respectively. Proton chemical shifts (δ) are relative to tetramethylsilane (TMS, $\delta = 0.0$) as internal standard and expressed in parts per million (ppm). Spin multiplicities were given as s (singlet), d (doublet), t (triplet), (qt) quartet, dd (doublet of doublet), dt (doublet of triplet),

ddd (doublet of doublet of doublet) and m (multiplet). Coupling constants (J) are given in Hertz (Hz). The assignment of protons and carbons were done using two-dimensional spectroscopic techniques COSY, HMQC and HMBC. IR spectra were recorded using IR Prestige-21 (Shimadzu) spectrometer. Melting points were determined by using SMP-30 melting point apparatus (Stuart Scientific, Staffordshire, UK). Elemental analyses were done on Elementar, vario MICRO cube elemental analyzer (Elementar Americas, Ronkonkoma, NY, USA). Ion-exchange chromatography was performed on Biologic DuoFlow (Bio-Rad, Hercules, CA, USA) by using Q-Sepharose as Fast Flow resin, 2 M triethylammonium bicarbonate (TEAB) buffer and MilliQ water were used as gradient solvents. Phosphate analysis was done using Briggs and Ames phosphate assays. X-ray intensity data measurements of freshly grown crystals were carried out at 298K on a Bruker-KAPPA APEX II CCD (Bruker, Mannheim, Germany) diffractometer with graphite monochromatized (MoK = 0.71073 Å) radiation. The X-ray generator was operated at 50 kV and 30 mA. Data were collected with scan width of 0.3° at different settings of φ (0°, 90° and 180°), keeping the sample to detector distance fixed at 40 mm. The X-ray data collection was monitored by SMART program (Bruker, 2003) [64]. All the data were corrected for Lorentzian, polarization and absorption effects using SAINT and SADABS programs (Bruker, 2003). SHELX-97 was used for structure solution and full matrix least-squares refinement on F2 [65]. All the hydrogen atoms were placed in geometrically idealized position and refined in the riding model approximation with C-H = 0.95 Å, and with Uiso (H) set to 1.2Ueq (C). Molecular diagrams were generated using ORTEP. Geometrical calculations were performed using SHELXTL (Bruker, 2003) and PLATON. Statistical analysis was performed using GraphPad Prism 5 (GraphPad Software, San Diego, CA, USA). Results are represented as mean \pm SEM. The differences between multiple groups were analyzed by one-way ANOVA, using Tukey's multiple comparison test. $p \leq 0.05$ is treated as statistically significant.

3.2. Synthesis

3.2.1. Synthesis of *Scyllo*-Inositol (2)

To a solution of compound **1** [45] (1 g, 2.33 mmol) in ethanol (15 mL), 1 N HCl solution (5 mL) was added and refluxed for 1h. After completion of the reaction, the reaction mass was filtered and the resultant solid was washed with DCM, and dried under reduced pressure, to get compound **2** (0.3 g, 72%) as a white solid. ¹H-NMR of compound **2** was identical with the reported data [46].

3.2.2. Synthesis of 1,2,3,4,5,6-Hexakis-*O*-(dibenzoyloxyphosphoryl)-*Scyllo*-Inositol (3)

Dibenzyl *N,N*-diisopropylphosphoramidite (2.3 g, 6.66 mmol) was added to a mixture of *scyllo*-inositol (**2**) (100 mg, 0.55 mmol) and 1*H*-tetrazole (0.46 g, 6.66 mmol) in acetonitrile (10 mL). The mixture was stirred for 15 h at room temperature. After 15 h, temperature of the reaction mixture was cooled down to -78 °C, then *m*-CPBA (1.3 g, 8.3 mmol) was added and the reaction mixture was slowly warmed to room temperature. The reaction mass was extracted with ethyl acetate and washed successfully with sat. aq. Na₂SO₃, sat. aq. NaHCO₃, water and brine. The organic layer was dried over anhydrous Na₂SO₄ and the solvent was evaporated under reduced pressure. The crude product thus obtained was purified by column chromatography using ethyl acetate and petroleum ether (1:1, *v/v*) as eluent, to get compound **3** (380 mg, 0.22 mmol, 40%) as sticky liquid. ¹H and ³¹P-NMR of compound **3** were identical with the reported data [46].

3.2.3. Synthesis of *Scyllo*-Inositol Hexakisphosphate (4)

To a solution of 1,2,3,4,5,6-hexakis-*O*-(dibenzoyloxyphosphoryl)-*scyllo*-inositol (**3**) (320 mg, 0.18 mmol) in a mixture of MeOH/H₂O (2:1, *v/v*, 10 mL), 10% Pd/C (100 mg) was added at room temperature and stirred under hydrogen atmosphere (using balloon) for 10 h. After completion of the reaction, the reaction mass was filtered through a PTFE filter and the filtrate was concentrated under reduced pressure. Then, the residue was purified by ion-exchange chromatography on Q-sepharose Fast Flow resin eluting with a gradient of

aqueous TEAB (0 to 1.0 M) to obtain the triethylammonium salt of *scyllo*-inositol hexakisphosphate (**4**, 104 mg, 0.16 mmol, 89%) as a white foamy solid. ^1H and ^{31}P -NMR of the compound were identical with the reported data [46].

3.2.4. Synthesis of 6-*O*-Benzoyl-2,4-Di-*O*-(*p*-Methoxybenzyl)-1,3,5-*O*-Methylidene-*Scyllo*-Inositol (**5**)

To a solution of compound **1** (1 g, 2.33 mmol) in dry pyridine (20 mL) at 0 °C, benzoyl chloride (0.4 mL, 3.48 mmol) and DMAP (50 mg, 0.41 mmol) were added and stirred for 4–5 h. After completion of the reaction, water was added to quench the excess benzoyl chloride. The crude reaction mass was extracted with ethyl acetate and then washed thoroughly with saturated NaHCO_3 solution, water and brine. The organic layer was dried over anhydrous Na_2SO_4 and the solvent was evaporated under reduced pressure. The crude product thus obtained was purified by column chromatography using ethyl acetate and petroleum ether (2:8, *v/v*) as eluent, to get compound **5** (1.2 g, 96%) as a white solid. The m. p. = 92 °C; RF = 0.7 (ethyl acetate/petroleum ether, 3:7, *v/v*); ^1H -NMR (500 MHz, CDCl_3) δ : 3.69 (s, 6H, 2 x OCH_3), 4.31 (brs, 2H), 4.37 (d, $J = 10.4$ Hz, 2H, ArCH_2), 4.48 (d, $J = 10.4$ Hz, 2H, ArCH_2), 4.56 (brs, 3H), 5.52 (s, 1H), 5.57 (brs, 1H), 6.59 (d, $J = 8.2$ Hz, 4H, ArH), 6.96–7.0 (m, 6H, ArH), 7.33 (t, $J = 7.4$ Hz, 1H, ArH), 7.74 (d, $J = 7.7$ Hz, 2H, ArH). ^{13}C -NMR (CDCl_3 , 125 MHz) δ : 55.2, 66.6, 67.9, 68.4, 71.6 (ArCH_2), 72.7, 103.1, 113.6, 128.0, 128.5, 129.5, 129.6, 129.62, 130.2, 130.3, 132.8, 159.1, 166.1. Elemental analysis Calcd for $\text{C}_{30}\text{H}_{30}\text{O}_9$: C, 67.41; H, 5.66. Found C, 67.23; H, 5.75.

3.2.5. Synthesis of 1-*O*-Benzoyl-*Scyllo*-Inositol (**6**)

To a solution of compound **5** (1.0 g, 1.87 mmol) in ethanol (15 mL), 1 N HCl (5 mL) was added and refluxed for 1h. After completion of the reaction, the reaction mass was filtered and the obtained solid was washed with DCM and dried under reduced pressure to get compound **6** as a white solid (0.42 g, 79%). ^1H -NMR of compound **6** was identical with the reported data [46].

3.2.6. Synthesis of 6-*O*-Benzoyl-1,2,3,4,5-Pentakis-*O*-(Dibenzoyloxyphosphoryl)-*Scyllo*-Inositol (**7**)

Dibenzyl *N,N*-diisopropylphosphoramidite (0.49 g, 1.41 mmol) was added to a mixture of 1-*O*-benzoyl-*scyllo*-inositol (**6**) (40 mg, 0.14 mmol) and 1*H*-tetrazole (99 mg, 1.41 mmol) in dry acetonitrile (10 mL). The mixture was stirred for 15 h at room temperature. After 15 h, temperature of the reaction mixture was cooled down to -78 °C, then *m*-CPBA (60%, 0.33 g, 2.1 mmol) was added and the reaction mixture was slowly warmed to room temperature. The reaction mass was extracted with ethyl acetate and washed successfully with sat. aq. Na_2SO_3 , sat. aq. NaHCO_3 , water and brine. The organic layer was dried over anhydrous Na_2SO_4 and the solvent was evaporated under reduced pressure. The crude product thus obtained was purified by column chromatography using ethyl acetate and petroleum ether (1:1, *v/v*) as eluent, to get compound **7** (0.2 g, 0.13 mmol, 93%) as a sticky liquid; ^1H -NMR (500 MHz, CDCl_3) δ : 4.46 (dd, $J = 9.3$ Hz, 11.7 Hz, 2H, ArCH_2), 4.67 (d, $J = 7.4$ Hz, 1H, ArCHA), 4.70 (d, $J = 7.4$ Hz, 1H, ArCHB), 4.74 (d, $J = 8.1$ Hz, 1H, ArCHA), 4.76 (d, $J = 8.1$ Hz, 1H, ArCHB), 5.01–4.77 (m, 19H, ArCH_2 & H-2, H-3, H-4, H-5, H-6), 5.69 (t, $J = 7.6$ Hz, 1H, H-1), 6.85 (m, 4H, ArH), 6.98 (m, 4H, ArH), 7.05–7.23 (m, 42H, ArH), 7.23 (t, $J = 7.9$ Hz, 1H, ArH), 7.42–7.38 (td, $J = 1.2$ Hz, 7.5 Hz, 1H, ArH), 7.98 (dd, $J = 1.2$ Hz, 8.3 Hz, 1H, ArH). ^{13}C -NMR (CDCl_3 , 125 MHz) δ : 69.4, 69.5, 69.6, 69.7, 69.9, 69.92, 69.97, 70.0, 70.04, 72.1, 75.9 (^{31}P coupled), 76.3 (^{31}P coupled), 127.7, 127.9, 128.1, 128.15, 128.2, 128.28, 128.31, 128.35, 128.4, 128.42, 128.44, 129.3, 130.2, 133.2, 135.3, 135.37, 135.6, 135.66, 135.7, 165.2. ^{31}P -NMR (202.4 MHz, CDCl_3) δ : -1.77 (2P), -1.84 (3P). Elemental analysis Calcd for $\text{C}_{83}\text{H}_{81}\text{O}_{22}\text{P}_5$: C, 62.88; H, 5.15. Found C, 62.76; H, 5.32.

3.2.7. Synthesis of 6-*O*-Benzoyl-*Scyllo*-Inositol-1,2,3,4,5-Pentakisphosphate (**8**)

To a solution of 6-*O*-benzoyl-1,2,3,4,5-pentakis-*O*-(dibenzoyloxyphosphoryl)-*scyllo*-inositol (**7**) (160 mg, 0.1 mmol) in a mixture of MeOH/ H_2O (2:1, *v/v*, 15 mL), 10% Pd/C (50 mg)

was added at room temperature and stirred under hydrogen atmosphere (using balloon) for 10 h. After completion of the reaction, the reaction mass was filtered through a PTFE filter and the filtrate was concentrated under reduced pressure. Then the residue was purified by ion-exchange chromatography on Q-sepharose Fast Flow resin eluting with a gradient of aqueous TEAB (0 to 1.0 M) to obtain the triethylammonium salt of 1-*O*-benzoyl-*scyllo*-inositol-2,3,4,5,6-pentakisphosphate (**8**) (50 mg, 0.073 mmol, 73%) as a white foam; $^1\text{H-NMR}$ (500 MHz, CDCl_3) δ : 4.44–4.36 (m, 3H, H-3,H-4, H-5), 4.51 (qt, $J = 9.3$ Hz, 2H, H-2, H-6), 5.53 (t, $J = 9.6$ Hz, 1H, H-1), 7.4 (t, $J = 7.4$ Hz, 2H, ArH), 7.53 (t, $J = 7.5$ Hz, 1H, ArH), 7.95 (t, $J = 7.9$ Hz, 2H, ArH). $^{13}\text{C-NMR}$ (CDCl_3 , 125 MHz) δ : 71.8 (C-1), 75.3 (C-2, C-6), 76.3 (C-4), 76.4 (C-3, C-5), 128.5, 128.9, 129.8, 133.9, 167.7. $^{31}\text{P-NMR}$ (202.4 MHz, CDCl_3) δ : 2.12 (1P), 1.91 (2P), 1.61 (2P). Elemental analysis Calcd for $\text{C}_{13}\text{H}_{21}\text{O}_{22}\text{P}_5$: C, 22.82; H, 3.09. Found C, 22.75; H, 3.33.

3.2.8. Synthesis of *Scyllo*-Inositol-1,2,3,4,5-Pentakisphosphate (**9**)

The 1 N LiOH (5 mL) was added to 6-*O*-benzoyl-*scyllo*-inositol-1,2,3,4,5-pentakisphosphate (**8**) (50 mg, 0.073 mmol) and heated at 80 °C for 3 h. After completion of the reaction the reaction mass was passed through Dowex 50WX8-100 (H+ form) and eluted with water. The filtrate was concentrated under reduced pressure to obtain compound **9** (34 mg, 0.058 mmol, 80%) as a sticky solid. ^1H and ^{31}P -NMR of the compound were identical with the reported data [46].

3.2.9. Synthesis of 1-*O*-*p*-Methoxybenzyl-3,4,5,6-Tetra-*O*-Benzoyl-*Myo*-Inositol (**11**)

To a solution of 1,4,5,6-tetra-*O*-benzoyl-*myo*-inositol (**10**) [50] (7 g, 11.7 mmol) in dry acetonitrile (150 mL), dibutyltin oxide (3.2 g, 12.87 mmol) and tetrabutylammonium bromide (6.49 g, 17.6 mmol) were added at room temperature and the mixture was refluxed for 3–4 h. The reaction mass was then brought to room temperature, *p*-methoxybenzylchloride (2.76 g, 17.6 mmol) was added and heated at 60 °C for 12 h. After completion of the reaction, Et_3N (1.18 g, 23.4 mmol) was added and refluxed for 1 h. Then the reaction mass was extracted with ethyl acetate, washed successively with sat. aq. NaHCO_3 solution, water and brine. The organic layer was dried over anhydrous Na_2SO_4 and the solvent was evaporated under reduced pressure. The crude product thus obtained was purified by column chromatography using a mixture of ethyl acetate and petroleum ether (3:7, *v/v*) as eluent, to get compound **11** (7.04 g, 9.82 mmol, 84%) as a white solid. The m. p. = 188 °C; $R_f = 0.6$ (ethyl acetate/petroleum ether, 3:7, *v/v*); $^1\text{H-NMR}$ (500 MHz, CDCl_3) δ : 2.73 (s, 1H, 2-OH), 3.67 (s, 3H, OCH_3), 3.82 (dd, $J = 2.2$ Hz, 9.75 Hz, 1H, H-1), 4.40 (d, $J = 11.8$ Hz, 1H, CH_2), 4.58 (m, 2H, Ar CH_2 & H-2), 5.23 (dd, $J = 1.9$ Hz, 10.3 Hz, 1H, H-3), 5.70 (t, $J = 10$ Hz, 1H, H-5), 5.98 (t, $J = 9.9$ Hz, 1H, H-6), 6.23 (t, $J = 10.2$ Hz, 1H, H-4), 6.59 (d, $J = 6.6$ Hz, 2H, ArH of PMB), 7.0 (d, $J = 8.5$ Hz, 2H, ArH of PMB), 7.21 (m, 3H), 7.34–7.29 (m, 7H), 7.47–7.43 (m, 2H), 7.70 (t, $J = 7.6$ Hz, 4H), 7.82 (d, $J = 7.3$ Hz, 2H), 7.93 (d, $J = 7.3$ Hz, 2H). $^{13}\text{C-NMR}$ (CDCl_3 , 125 MHz) δ : 55.2, 67.4 (C-2), 69.8 (C-4), 71.2 (C-5), 71.3 (C-6), 71.9 (Ar CH_2), 72.1 (C-3), 76.3 (C-1), 113.9, 128.2, 128.3, 128.5, 128.7, 128.8, 129.0, 129.2, 129.5, 129.6, 129.72, 129.76, 129.8, 129.9, 133.0, 133.1, 133.2, 133.5, 159.6, 165.4, 165.5, 165.8, 166.0. Elemental analysis Calcd for $\text{C}_{42}\text{H}_{36}\text{O}_{11}$: C, 70.38; H, 5.06. Found C, 70.49; H, 4.82.

3.2.10. Synthesis of 1-*O*-*p*-Methoxybenzyl-3,4,5,6-Tetra-*O*-Benzoyl-2-*O*-Trifluoromethanesulfonyl-*Myo*-Inositol (**12**)

To a solution of 1-*O*-*p*-methoxybenzyl-3,4,5,6-tetra-*O*-benzoyl-*myo*-inositol (**11**) (7.0 g, 9.76 mmol) in a mixture of dry DCM (50 mL) and dry pyridine (20 mL), triflic anhydride (5.51 g, 19.5 mmol) was added at 0 °C. After completion of the reaction, reaction mass was extracted with DCM and the organic layer was washed successfully with sat. aq. NaHCO_3 , water and brine. The organic layer was dried over anhydrous Na_2SO_4 and the solvent was evaporated under reduced pressure. The crude product thus obtained was purified by column chromatography using a mixture of ethyl acetate and petroleum ether (2:8, *v/v*) as eluent, to get compound **12** (5.38 g, 6.34 mmol, 65%) as a white solid; m. p. = 126 °C; ^{19}F

NMR (470 MHz, CDCl₃) δ : -76.0. ¹H-NMR (500 MHz, CDCl₃) δ : 3.68 (s, 3H, OCH₃), 3.97 (dd, J = 1.9 Hz, 10.2 Hz, 1H, H-1), 4.34 (d, J = 12.2 Hz, 1H, ArCH_A), 4.70 (d, J = 12.2 Hz, 1H, ArCH_B), 5.44 (dd, J = 2.1 Hz, 10.5 Hz, 1H, H-3), 5.59 (brs, 1H, H-2), 5.72 (t, J = 10.1 Hz, 1H, H-5), 5.89 (t, J = 10.1 Hz, 1H, H-6), 6.09 (t, J = 10.27 Hz, 1H, H-4), 6.58 (d, J = 8.5 Hz, 2H, ArH of PMB), 7.0 (d, J = 8.5 Hz, 2H, ArH of PMB), 7.17–7.21 (m, 1H), 7.29–7.35 (m, 8H), 7.47 (m, 3H), 7.73 (t, J = 6.9 Hz, 4H), 7.78 (d, J = 7.3 Hz, 2H), 7.92 (d, J = 7.3 Hz, 2H). ¹³C-NMR (CDCl₃, 125 MHz) δ : 55.0, 55.2, 69.2 (C-3), 69.3 (C-4), 70.1 (C-6), 70.6 (C-5), 72.0 (ArCH₂), 72.9 (C-1), 82.0 (C-2), 113.9, 127.8, 128.0, 128.3, 128.4, 128.5, 128.6, 129.1, 129.7, 129.8, 129.9, 130.0, 130.1, 133.3, 133.36, 133.4, 134.0, 159.7, 164.9, 165.1, 165.6, 165.7. Elemental analysis Calcd. for C₄₃H₃₅F₃O₁₃S: C, 60.85; H, 4.16. Found C, 60.68; H, 4.11.

3.2.11. Synthesis of 2-O-Acetyl-1-O-*p*-Methoxybenzyl-3,4,5,6-Tetra-O-Benzoyl-Scyllo-Inositol (**13**)

To a solution of 1-*O-p*-methoxybenzyl-3,4,5,6-tetra-*O*-benzoyl-2-*O*-trifluoromethanesulfonyl-*myo*-inositol (**12**) (5 g, 5.89 mmol) in *N,N*-dimethylacetamide (30 mL), potassium acetate (2.89 g, 29.5 mmol) was added and heated at 70 °C for 2 h. After completion of the reaction, the reaction mass was extracted with ethyl acetate and thoroughly washed with water and brine. The organic layer was dried over anhydrous Na₂SO₄ and the solvent was evaporated under reduced pressure. The crude product thus obtained was purified by column chromatography using a mixture of ethyl acetate and petroleum ether (2:8, *v/v*) as eluent, to get compound **13** (4.25 g, 5.59 mmol, 95%) as a white solid; m. p. = 254 °C; ¹H-NMR (500 MHz, CDCl₃) δ : 1.83 (s, 3H, OAc), 3.64 (s, 3H, OCH₃), 3.99 (t, J = 9.2 Hz, 1H, H-1), 4.47 (d, J = 11.8 Hz, 1H, ArCH_A), 4.52 (d, J = 11.7 Hz, 1H, ArCH_B), 5.55 (t, J = 9.7 Hz, 1H, H-6), 5.65 (t, J = 9.7 Hz, 1H, H-5), 5.82–5.71 (m, 3H, H-2, H-3, H-4), 6.59 (d, J = 8.5 Hz, 2H, ArH of PMB), 6.96 (d, J = 8.5 Hz, 2H, ArH of PMB), 7.33–7.27 (m, 7H), 7.46–7.42 (m, 2H), 7.70 (d, J = 7.5 Hz, 4H), 7.82 (t, J = 6.6 Hz, 4H). ¹³C-NMR (CDCl₃, 125 MHz) δ : 20.6, 55.2, 70.6 (C-2 or C-3 or C-4 or C-5), 70.7 (C-3 or C-4 or C-5 or C-2), 71.0 (C-4 or C-5 or C-2 or C-3), 71.9 (C-6), 72.2 (C-5 or C-2 or C-3 or C-4), 74.5 (ArCH₂), 77.2 (C-1), 113.7, 128.2, 128.3, 128.4, 128.5, 128.6, 128.7, 129.1, 129.2, 129.7, 129.8, 129.9, 133.2, 133.3, 133.5, 159.3, 165.2, 165.3, 165.5, 165.6, 169.4. Elemental analysis Calcd. for C₄₄H₃₈O₁₂: C, 69.65; H, 5.05. Found C, 69.59; H, 4.83.

3.2.12. Synthesis of 1-*O-p*-Methoxybenzyl-Scyllo-Inositol (**14**)

To a solution of 2-*O*-acetyl-1-*O-p*-methoxybenzyl-3,4,5,6-tetra-*O*-benzoyl-*scyllo*-inositol (4.0 g, 5.27 mmol) in methanol (50 mL), sodium methoxide (57 mg, 1.05 mmol) was added and refluxed for 4 h. After completion of the reaction, Dowex[®] 50WX8 H⁺ (1 g) was added to the reaction mass and stirred at room temperature for 10 min. Then, the mixture was filtered and the resin was washed with methanol. The combined filtrate was evaporated under reduced pressure to get the title compound **14** as a white solid (1.55 g, 5.16 mmol, 98%). Charred at 220 °C without melting; ¹H-NMR (500 MHz, CDCl₃) δ : 2.94–3.04 (m, 4H), 3.12–3.17 (m, 2H), 3.73 (s, 3H, OCH₃), 4.69 (s, 2H, ArCH₂), 4.81 (brs, 5H, OH), 6.86 (d, J = 8.5 Hz, 2H, ArH), 7.33 (d, J = 8.5 Hz, 2H, ArH). ¹³C-NMR (CDCl₃, 125 MHz) δ : 55.5, 73.7, 74.4, 74.5, 74.8, 83.3, 113.7, 129.6, 132.2, 158.8. Elemental analysis Calcd for C₁₄H₂₀O₇: C, 55.99; H, 6.71. Found C, 55.82; H, 6.65.

3.2.13. Synthesis of 6-*O-p*-Methoxybenzyl-1,2,3,4,5-Pentakis-*O*-(Dibenzoyloxyphosphoryl)-Scyllo-Inositol (**15**)

Dibenzyl *N,N*-diisopropylphosphoramidite (5.76 g, 16.7 mmol) was added to a solution of 1-*O-p*-methoxybenzyl-*scyllo*-inositol (**14**) (0.5 g, 1.67 mmol) and 1*H*-tetrazole (1.17 g, 16.7 mmol) in dry acetonitrile (30 mL). The mixture was stirred for 15 h at room temperature. After 15 h, the reaction mixture was cooled down to -78 °C, then *m*-CPBA (3.92 g, 25.05 mmol) was added and the reaction mixture was slowly warmed to room temperature. The reaction mass was extracted with ethyl acetate and washed successively with sat. aq. Na₂SO₃, sat. aq. NaHCO₃, water and brine. The organic layer was dried over anhydrous Na₂SO₄ and the solvent was evaporated under reduced pressure. The crude product thus

obtained was purified by column chromatography using a mixture of ethyl acetate and petroleum ether (1:1, *v/v*) as eluent, to get compound **15** (2.4 g, 15.03 mmol, 90%) as a sticky liquid. $^1\text{H-NMR}$ (500 MHz, CDCl_3) δ : 3.56 (s, 3H, OCH_3), 4.06 (t, $J = 4.5$ Hz, 1H), 4.4 (brs, 2H), 4.80–4.99 (m, 25H), 6.56 (d, $J = 8.5$ Hz, 2H), 7.1–7.2 (m, 52H). $^{13}\text{C-NMR}$ (CDCl_3 , 125 MHz) δ : 55.1, 69.6, 69.7, 69.8, 69.9, 72.5, 76.9 (^{31}P coupled), 77.3 (^{31}P coupled), 79.3 (^{31}P coupled), 113.6, 128.0, 128.1, 128.3, 128.4, 128.5, 129.3, 129.5, 135.57, 135.63, 135.65, 135.68, 135.7, 135.71, 135.73, 159.1. $^{31}\text{P-NMR}$ (202.4 MHz, CDCl_3) δ : -1.9 , -2.0 . Elemental analysis Calcd for $\text{C}_{84}\text{H}_{85}\text{O}_{22}\text{P}_5$: C, 63.00; H, 5.35. Found C, 62.82; H, 5.61.

3.2.14. Synthesis of 1,2,3,4,5-Pentakis-*O*-(Dibenzoyloxyphosphoryl)-*Scyllo*-Inositol (**16**)

To a solution of 6-*O*-*p*-methoxybenzyl-1,2,3,4,5-pentakis-*O*-(dibenzoyloxyphosphoryl)-*scyllo*-inositol (**15**) (1 g, 0.62 mmol) in anhydrous 1,2-dichloroethane (20 mL), DDQ (170.0 mg, 0.75 mmol) was added and heated at 60 °C for 3–4 h. After completion of the reaction, the reaction mass was concentrated under reduced pressure and the crude residue was purified by column chromatography using a mixture of ethyl acetate and petroleum ether (1:1, *v/v*) as eluent to get compound **16** (670 mg, 0.45 mmol, 73%) as a white solid. The m. p. = 112 °C; $^1\text{H-NMR}$ (500 MHz, CDCl_3) δ : 3.98 (td, $J = 2.5$ Hz, 8.2 Hz, 1H, H-1), 4.65 (qt, $J = 8.1$ Hz, 2H, H-2 & H-6), 4.65 (m, 1H, H-4), 4.73 (qt, $J = 7.8$ Hz, 2H, H-3 & H-5), 4.91–5.13 (m, 20H), 5.29 (d, $J = 2.6$ Hz, 1H, OH-1), 7.15–7.29 (m, 50H). $^{13}\text{C-NMR}$ (CDCl_3 , 125 MHz) δ : 69.64, 69.68, 69.72, 69.77, 69.85, 69.89, 69.96, 70.01, 70.05, 70.09, 72.4 (C-1), 75.4 (C-4, ^{31}P coupled), 75.9 (C-3 & C-5, ^{31}P coupled), 79.1 (C-2 & C-6, ^{31}P coupled), 127.9, 128.03, 128.07, 128.1, 128.3, 128.33, 128.38, 128.4, 128.47, 128.5, 135.5, 135.62, 135.69, 135.71, 135.76, 135.8, 135.86. $^{31}\text{P-NMR}$ (202.4 MHz, CDCl_3) δ : -1.55 , -1.50 , -0.79 . Elemental analysis Calcd for $\text{C}_{76}\text{H}_{77}\text{O}_{21}\text{P}_5$: C, 61.62; H, 5.24. Found C, 61.85; H, 4.87.

3.2.15. Crystal Data for **16**

CCDC No. 1946543 (Figure 7) Molecular formula = $\text{C}_{76}\text{H}_{77}\text{O}_{21}\text{P}_5$, Formula weight = 1481.23, colorless blocks, $0.25 \times 0.20 \times 0.15$ mm, Triclinic, space group P-1, 12.9915(9), $b = 16.3817(11)$, $c = 19.4914(14)$ Å, $V = 3759.2(5)$ Å³, $Z = 2$, $T = 293(2)$ K, $2\theta_{\text{max}} = 50.00^\circ$, $D_{\text{calc}} (\text{g cm}^{-3}) = 1.309$, $F(000) = 1552$, $\mu (\text{mm}^{-1}) = 0.194$, 55445 reflections measured, 13192 unique reflections ($R_{\text{int}} = 0.0907$), multi-scan absorption correction, $T_{\text{min}} = 0.9530$, $T_{\text{max}} = 0.9714$, number of parameters = 847, number of restraints = 396, $\text{GoF} = 0.986$, $R1 = 0.0884$, $wR2 = 0.2343$, R indices based on 13192 reflections with $I > 2s(I)$. $\Delta\rho_{\text{max}} = 0.555$, $\Delta\rho_{\text{min}} = -0.358$ ($\text{e}\text{\AA}^{-3}$).

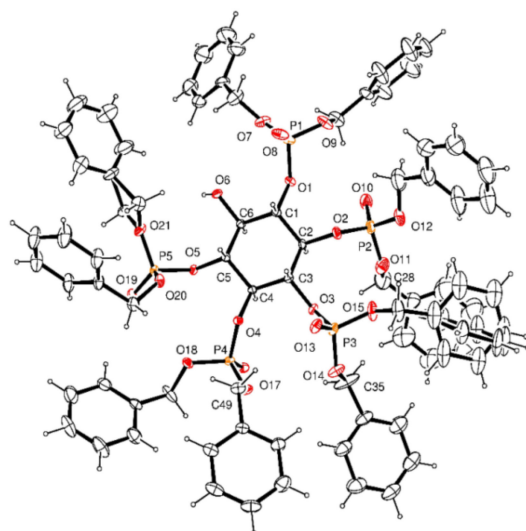
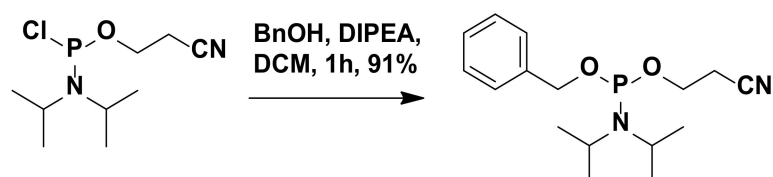


Figure 7. ORTEP diagram of compound **16** at 30% probability level.

3.2.16. Synthesis of 2-Cyanoethyl-*N,N*-Diisopropylbenzylphosphoramidite

Diisopropylethylamine (0.87 mL, 5.0 mmol) was added to a mixture of chloro-2-cyanoethyl-*N,N*-diisopropylphosphoramidite (1.1 mL, 5.0 mmol) and benzyl alcohol (0.52 mL, 5.0 mmol) at room temperature and stirred for 1 h (Scheme 3). The reaction mixture was extracted with DCM, washed with sat. aq. NaHCO₃ and the organic layer was dried over anhydrous Na₂SO₄. The organic layer was concentrated under reduced pressure and used without any further purification. ¹H and ³¹P-NMR of the compound (1.4 g, 4.54 mmol, 91%) were identical with the reported data [66].



Scheme 3. Synthesis of 2-Cyanoethyl-*N,N*-Diisopropylbenzylphosphoramidite.

3.2.17. Synthesis of 6-((Benzyloxy)(2-Cyanoethoxy)Phosphoryl)-1,2,3,4,5-Pentakis-*O*-(Dibenzyloxyphosphoryl)-*Scyllo*-Inositol (**17**)

To a solution of 1,2,3,4,5-pentakis-*O*-(dibenzyloxyphosphoryl)-*scyllo*-inositol (**16**) (0.2 g, 0.135 mmol) in dry DCM (10 mL), 2-cyanoethyl *N,N*-diisopropylbenzylphosphoramidite (0.41 g, 1.35 mmol) and 1*H*-tetrazole (0.094 g, 1.35 mmol) were added. The mixture was stirred for 4 h at room temperature and then *m*-CPBA (0.32 g, 2.03 mmol) was added at −78 °C and the reaction mixture was slowly warmed to room temperature. The reaction mass was then extracted with ethyl acetate and washed successively with sat. aq. Na₂SO₃, sat. aq. NaHCO₃, water and brine. The organic layer was dried over anhydrous Na₂SO₄ and the solvent was evaporated under reduced pressure. The crude product thus obtained was purified through column chromatography using a mixture of acetone and petroleum ether (3:7, *v/v*) as eluent, to get compound **17** (160 mg, 0.09 mmol, 67%) as a sticky liquid; ¹H-NMR (500 MHz, CDCl₃) δ: 2.29 (t, *J* = 6.4 Hz, 2H), 3.93 (m, 2H), 4.87–5.08 (m, 28H), 7.12–7.20 (m, 55H). ¹³C-NMR (CDCl₃, 125 MHz) δ: 62.4, 62.5, 69.9, 70.0, 70.1, 70.3, 70.4, 76.3, 76.4, 116.6, 128.0, 128.11, 128.19, 128.3, 128.5, 128.52, 128.6, 128.66, 128.7, 128.8, 135.2, 135.3, 135.52, 135.58. ³¹P-NMR (202.4 MHz, CDCl₃) δ: −1.98, −2.78. Elemental analysis Calcd for C₈₆H₈₇NO₂₄P₆: C, 60.60; H, 5.14; N, 0.82. Found C, 60.53; H, 5.27; N, 0.88.

3.2.18. Synthesis of 6-*O*-Benzyloxyphosphoryl-1,2,3,4,5-Pentakis-*O*-(Dibenzyloxyphosphoryl)-*Scyllo*-Inositol (**18**)

To a solution of 6-((benzyloxy)(2-cyanoethoxy)phosphoryl)-1,2,3,4,5-pentakis-*O*-(dibenzyloxyphosphoryl)-*scyllo*-inositol (**17**) (0.1 g, 0.059 mmol) in dry acetonitrile (1.0 mL), DBU (35 μL, 0.24 mmol) was added followed by the addition of bis(trimethylsilyl)trifluoroacetamide (0.5 mL) under nitrogen atmosphere. After 1 h, the reaction mixture was filtered through Dowex-H⁺ resin. The filtrate was concentrated under reduced pressure and the crude reaction mass was purified by column chromatography using methanol and dichloromethane (1:9, *v/v*) as eluent to afford compound **18** (88 mg, 0.053 mmol, 90%) as a sticky solid; ¹H-NMR [500 MHz, CDCl₃:CD₃OD (3:1)] δ: 1.61–1.70 (m, 5H), 2.48–2.50 (m, 2H), 3.31–3.37 (m, 4H), 3.75 (m, 1H), 4.77–4.88 (m, 24H), 4.93 (m, 2H), 5.17 (m, 2H), 6.99–7.13 (m, 55H). ¹³C-NMR (CDCl₃:CD₃OD (3:1), 125 MHz) δ: 23.1, 26.5, 28.1, 29.7, 31.8, 36.1, 36.7, 45.3, 49.9, 67.6, 67.7, 69.8, 69.9, 69.98, 70.0, 70.2, 70.3, 70.36, 70.4, 74.7 (³¹P coupled), 76.8 (³¹P coupled), 77.0 (³¹P coupled), 77.5 (³¹P coupled), 112.4, 114.6, 117.0, 119.2, 127.3, 127.4, 127.9, 127.98, 128.0, 128.1, 128.3, 128.4, 128.47, 134.9, 135.0, 135.07, 135.2, 135.22, 135.26, 137.5, 159.1, 159.4, 159.7, 159.8, 160.0, 177.9. ³¹P-NMR (202.4 MHz, CDCl₃) δ: −1.92, −2.55, −3.03, −3.0. Elemental analysis Calcd for C₈₃H₈₄NO₂₄P₆: C, 60.37; H, 5.13. Found C, 60.31; H, 5.19.

3.2.19. Synthesis of 6-O-Diphospho-Scyllo-Inositol-1,2,3,4,5-Pentakisphosphate (Scyllo-IP7) (20)

To a solution of 6-O-benzyloxyphosphoryl-1,2,3,4,5-pentakis-O-(dibenzyloxyphosphoryl)-scyllo-inositol (**18**) (50 mg, 0.03 mmol) and trimethylamine (9 μ L, 0.06 mmol) in anhydrous DCM, dibenzylphosphoryl chloride (0.18 mL, 10% in toluene, 0.06 mmol) was added at 0 °C. After 2 h, the solvents were removed by applying vacuum, and the residue was completely dried at 10^{-2} mbar. The residue (**19**) was dissolved in *t*-BuOH/H₂O (6:1, *v/v*, 14 mL) to which 10% Pd/C (100 mg) was added and stirred under hydrogen atmosphere (balloon pressure) for 10 h. The catalyst was removed by filtration through a PTFE syringe filter and the filtrate was concentrated under reduced pressure. The obtained residue was purified by ion-exchange chromatography on Q-sepharose Fast Flow resin eluting with a gradient of triethylammonium bicarbonate (TEAB) buffer (0 to 2.0 M) and water to obtain the triethylammonium salt of **20** (10 mg, 44%) as a white solid. ³¹P-NMR (202.4 MHz, D₂O) δ : 1.99 (5P), -6.1 (1P), -11.0 (1P); HRMS (ESI) mass calculated for C₆H₁₉O₂₇P₇ [M - H]⁺, 738.8199, found 738.5057.

3.3. Generation and Detection of PPIP_n Products

The 6xHis-tagged mouse IP6K1 (mIP6K1) and GST-tagged kinase domain of *S. cerevisiae* Vip1 (amino acid residues 1–535) (GST-VIP1-KD) were expressed and purified as described earlier [67]. Assays to detect synthesis of PPIP_n product were set up in reaction buffer (20 mM Tris-Cl pH 7.4, 60 mM NaCl, 6 mM MgCl₂, 1 mM DTT) in a 25 μ L reaction volume for PAGE analysis and a 50 μ L reaction volume for HPLC analysis. For PAGE analysis, the reactions were supplemented with 1 mM Mg²⁺-ATP, an ATP regeneration system (6 mM phosphocreatine and 25 U/mL creatine phosphokinase), ~1.2 μ M purified enzyme, and either 200 μ M IP_n substrate (for 6xHis-IP6K1) or 100 μ M IP_n substrate (for GST-VIP1 KD), and were incubated at 37 °C for 18 h. The reactions were mixed with 0.1% orange G containing loading dye and were resolved on a 35.8 % polyacrylamide gel, overnight at 500 V in 1X TBE (Tris/borate/EDTA), as described earlier [52]. The gels were stained with 0.1% Toluidine blue (*w/v*) in 20% methanol and 2% glycerol and were destained in 20% methanol and 2% glycerol. The gels were scanned on a desktop scanner (Laserjet M1136 MFP).

For HPLC analysis, the reactions were supplemented with 1 mM Mg²⁺-ATP and 200 μ M IP_n substrate for 6xHis-mIP6K1, and 40 μ M Mg²⁺-ATP and 100 μ M IP_n substrate for GST-VIP1-KD. The concentration of ATP used in the assay was chosen on the basis of the reported affinities of IP6K1 and VIP1-kinase domain for ATP (K_m value for ATP for mIP6K1 is 1.1 mM [68]; K_m value for ATP has not been measured for *S. cerevisiae* VIP1, but the kinase domain of human PPIP5K2 has a K_m of 20–40 μ M for ATP [38]. All reactions contained 2.5 μ Ci [γ -³²P]ATP (Regional Centre Hyderabad, BRIT, India) and ~1.2 μ M purified enzyme, and were incubated at 37 °C for 18 h. A negative control was set up by incubating *myo*-IP₆ in the presence of ~1 μ M BSA, along with 2.5 μ Ci [γ -³²P] ATP and 40 μ M Mg²⁺-ATP. The reactions were terminated by the addition of 40 μ L of 6 mM EDTA, followed by 100 μ L of 0.6 M perchloric acid, followed by 33 μ L neutralization solution (1 M potassium carbonate and 5 mM EDTA). The inositol phosphates were resolved by HPLC (515 HPLC pumps, Waters) on a SAX Partisphere column (4.6 mm diameter and 125 mm length column, Whatman) using a gradient of buffer A (1 mM EDTA) and buffer B (1 mM EDTA and 1.3 M (NH₄)₂HPO₄, pH 3.8) as follows: 0–5 min, 0% B; 5–10 min, 0–20% B; 10–70 min, 20–100% B; 70–80 min, 100% B (see Supplementary Figure S2A for the elution gradient profile). One-milliliter fractions were mixed with 4 mL scintillation cocktail (Ultima-Flo AP, Perkin Elmer) and counted for 1 min in a liquid scintillation analyzer (Tri-Carb 2910 TR, Perkin Elmer). To identify the retention times for standard *myo*-IPs, we utilized radiolabelled inositol phosphates extracted from yeast strains harboring deletions of enzymes involved in inositol phosphate synthesis, as described earlier [69]. *S. cerevisiae* strain BY4741 wild type (WT), *ipk1* Δ , *kcs1* Δ and *vip1* Δ were grown in synthetic medium containing yeast nitrogen base with ammonium sulphate and without inositol (MP Biomedicals), 2% dextrose (Sigma-Aldrich), 76 mg/mL uracil (HiMedia Laboratories), synthetic

complete supplement mixture (SCSM; Formedium) without inositol, and supplemented with 5 $\mu\text{Ci}/\text{mL}$ of *myo*-2- ^{3}H inositol (15–20 Ci/mmol; American Radiolabeled Chemicals). The yeast was inoculated at OD_{600} 0.001 and grown to OD_{600} ~1.0 at 30 °C, harvested by centrifugation ($2000\times g$, 3 min), lysed in 350 μL chilled lysis buffer (1 M perchloric acid, 0.2 mg/mL IP_6 , 2 mM EDTA) by bead beating using glass beads (Sigma-Aldrich). The soluble cell extracts were harvested by centrifugation ($21,000\times g$ for 5 min) and neutralized with 1 M potassium carbonate/5 mM EDTA solution. The extracted inositol phosphates were resolved using the column and gradient described above. One-milliliter fractions were mixed with 3 mL scintillation cocktail and counted for 5 min, as described above. In this way, we were able to identify the retention time for *myo*- IP_5 , *myo*- IP_6 , *myo*-PP- IP_4 , *myo*-[PP] $_2$ - IP_3 , *myo*-PP- IP_5 and *myo*-[PP] $_2$ - IP_4 , based on the IP profile described earlier for these strains [70] (Supplementary Figure S2B). The retention time of $[\gamma\text{-}^{32}\text{P}]\text{ATP}$, determined from the negative control reaction (see Supplementary Figure S2C), was found to be ~20 min. Therefore, to avoid any carryover of ATP, fractions collected from 35–70 min of the elution gradient were monitored to identify the PPIP $_n$ product. Minor variations in column back-pressure during consecutive HPLC runs led to inter-assay variations in retention time. However, the column was calibrated for each experimental set by making a note of the retention time of 5PP-*myo* IP_4 , the product of *myo*- IP_5 formed in the presence of IP6K1 , and of 1PP-*myo*- IP_5 and 5PP-*myo*- IP_5 , the products of *myo*- IP_6 formed in the presence of VIP1-KD and IP6K1 , respectively, as indicated in Figure 2. The conversion of IP_n substrate (10 nmoles and 5 nmoles respectively for IP6K1 and VIP1-KD reactions) to PPIP $_n$ product (expressed in pmoles) was calculated based on the specific activity of ATP. All product peaks that were at least 5-fold above the baseline were counted. Data shown reflect the mean \pm S.E.M. from four independent assays, and were analyzed using GraphPad PRISM.

3.4. Detection and Quantification of ATP Consumed and ADP Generated during the Kinase/ATPase Reaction

To monitor ATP consumption by purified recombinant 6 \times His-m IP6K1 and GST-VIP1-KD, we used the ATPlite luminescence detection system (Perkin Elmer) as per the manufacturer's protocol. To rule out the possible co-purification of contaminating ATPases or phosphatases from the *E. coli* expression system, we used the generic ATPase inhibitor sodium orthovanadate (2 mM), or a mixture of phosphatase inhibitors (Phosphatase Inhibitor Cocktail 3, Sigma-Aldrich P0044, used at the recommended concentration). The reactions were set up with ~0.4 μM 6 \times His-m IP6K1 or ~0.2 μM GST-VIP1-KD in 1X reaction buffer (20 mM Tris-Cl pH 7.4, 60 mM NaCl, 6 mM MgCl_2 , and 1 mM DTT) in a final volume of 25 μL . *Bz-scyllo*- IP_5 (200 μM for IP6K1 and 100 μM for VIP1-KD) was used to stimulate the ATPase activity of the enzymes. The ATPase or phosphatase inhibitor, or a vehicle control, was added to the reaction for 15 min on ice, prior to the addition of ATP. The reactions were initiated by the addition of 40 μM Mg^{2+} -ATP, incubated for 1 h at 37 °C and suitably diluted for measurement of ATP. A standard curve was plotted with increasing amount of ATP and the luminescence values were extrapolated to obtain the amount of ATP remaining after the reaction was terminated. Data shown reflect the mean \pm range from two independent experiments and were analyzed using GraphPad PRISM.

The kinase/ATPase reactions for 6 \times His-m IP6K1 and GST-VIP1-KD were set up in reaction buffer in a 10 μL or 12.5 μL reaction volume, respectively. The reactions were supplemented with 1 mM ATP and 200 μM IP_n substrate for 6 \times His-m IP6K1 , and 40 μM ATP and 100 μM IP_n substrate for GST-VIP1-KD, and ~1.2 μM purified enzyme. The final amount of ATP in the reaction was 10 nmoles and 500 pmoles, respectively, for IP6K1 and Vip1 . Reactions were carried out for 18 h at 37 °C, cooled to 25 °C, and the amount of ADP generated was assayed using the ADP-GloTM kinase assay kit (Promega, Cat. # V6930), according to the manufacturer's protocol. The ADP-GloTM kinase assay is a luminescence-based ADP detection method to measure the amount of ADP generated in the kinase reaction, and also reflects non-productive ATPase activity. After completion of the kinase/ATPase reaction, an equal volume of ADP-GloTM reagent was added and incubated at 25 °C for 30 min to terminate the reaction and to deplete the remaining ATP.

The reaction mixture was transferred to a solid white 96-well plate, and double the volume of kinase detection reagent was added under dark, and incubated for 1 h to generate ATP from ADP, and measure the newly synthesized ATP using a luciferase/luciferin reaction. Luminescence was measured using a Multimode plate reader (EnSpire, Perkin Elmer, Waltham, MA, USA). The luminescence values were correlated with the percentage of ADP generated in the reaction by using an ATP-to-ADP standard curve. Appropriate volumes of ATP and ADP stock solutions were mixed to generate an ATP-to-ADP conversion standard curve. Separate standard curves were generated for IP6K1 and VIP1-KD—for IP6K1, 1 mM ATP and ADP solutions were mixed to obtain a range of ADP from 0% to 10% of ATP; and for Vip1, 40 μ M ATP and ADP solutions were mixed to obtain a range of ADP from 0% to 40% of ATP. In every sample used for the standard curve, we included 1X reaction buffer and 100 μ M or 200 μ M IP6 respectively for VIP1-KD or IP6K1 assays, to account for any effects of buffer components or IPns on the luminescence reading. Standard curves were plotted and data was interpolated from three independent assays each for IP6K1 and VIP1-KD. Data shown reflect the mean \pm S.E.M. from three independent assays, and were analyzed using GraphPad PRISM.

As shown in Figure 5, we observed significant basal ATPase activity without the addition of IPn substrate, especially in the case of VIP1-KD. The graphs shown in Figure 6 clearly depict the percentage ADP generated in the presence of IPn substrate, after subtracting the amount of ADP generated in the absence of substrate.

Supplementary Materials: The following are available online, Section S1. PAGE analysis of PPIPn products; Section S2. Calibration of SAX HPLC for resolution of IPs and PPIPs; Section S3. Molecular Docking; Section S4. Effect of inhibitors on ATPase activity of IP kinases; Section S5. Spectral data. References [52,69–75] are cited in the Supplementary Materials.

Author Contributions: Conceptualization, K.M.S. and R.B.; synthesis and characterization compounds, R.M. (Raja Mohanrao); biochemical assays, R.M. (Ruth Manorama) and S.G.; molecular docking, M.C.M.; preparation of the manuscript, R.M. (Raja Mohanrao), R.M. (Ruth Manorama), S.G., M.C.M., R.B. and K.M.S. All authors have read and agreed to the published version of the manuscript.

Funding: K.M.S. thanks the Department of Science and Technology, Govt. of India for a Swarna-Jayanti Fellowship. R.B. acknowledges support from the Science and Engineering Research Board, Department of Science and Technology, Govt. of India (CRG/2019/002597); Department of Biotechnology, Govt. of India (BT/PR29960/BRB/10/1762/2019); and CDFD core funds.

Institutional Review Board Statement: Not applicable.

Informed Consent Statement: Not applicable.

Data Availability Statement: The data presented in this study are available in the Supplementary Materials.

Acknowledgments: R.B. thanks members of the Laboratory of Cell Signalling for their valuable feedback.

Conflicts of Interest: The authors declare no conflict of interest.

Sample Availability: Some of the samples are available in small quantities. This may be available for some time.

References

1. Irvine, R.F.; Schell, M.J. Back in the water: The return of the inositol phosphates. *Nat. Rev. Mol. Cell Biol.* **2001**, *2*, 327–338. [[CrossRef](#)] [[PubMed](#)]
2. Best, M.D.; Zhang, H.; Prestwich, G.D. Inositol polyphosphates, diphosphoinositol polyphosphates and phosphatidylinositol polyphosphate lipids: Structure, synthesis, and development of probes for studying biological activity. *Nat. Prod. Rep.* **2010**, *27*, 1403–1430. [[CrossRef](#)]
3. Wilson, M.; Livermore, T.M.; Saiardi, A. Inositol pyrophosphates: Between signalling and metabolism. *Biochem. J.* **2013**, *452*, 369–379. [[CrossRef](#)]
4. Bennett, M.; Onnebo, S.M.N.; Azevedo, C.; Saiardi, A. Inositol pyrophosphates: Metabolism and signaling. *Cell. Mol. Life Sci.* **2006**, *63*, 552–564. [[CrossRef](#)] [[PubMed](#)]

5. Shah, A.; Ganguli, S.; Sen, J.; Bhandari, R. Inositol Pyrophosphates: Energetic, Omnipresent and Versatile Signalling Molecules. *J. Indian Inst. Sci.* **2017**, *97*, 23–40. [[CrossRef](#)]
6. Barker, C.J.; Illies, C.; Gaboardi, G.C.; Berggren, P.-O. Inositol pyrophosphates: Structure, enzymology and function. *Cell. Mol. Life Sci.* **2009**, *66*, 3851–3871. [[CrossRef](#)]
7. Shears, S.B.; Weaver, J.D.; Wang, H. Structural insight into inositol pyrophosphate turnover. *Adv. Biol. Regul.* **2013**, *53*, 19–27. [[CrossRef](#)] [[PubMed](#)]
8. Wang, H.; Gu, C.; Rolfes, R.J.; Jessen, H.J.; Shears, S.B. Structural and biochemical characterization of Siw14: A protein-tyrosine phosphatase fold that metabolizes inositol pyrophosphates. *J. Biol. Chem.* **2018**, *293*, 6905–6914. [[CrossRef](#)]
9. Auesukaree, C.; Tochio, H.; Shirakawa, M.; Kaneko, Y.; Harashima, S. Plc1p, Arg82p, and Kcs1p, Enzymes Involved in Inositol Pyrophosphate Synthesis, Are Essential for Phosphate Regulation and Polyphosphate Accumulation in *Saccharomyces cerevisiae*. *J. Biol. Chem.* **2005**, *280*, 25127–25133. [[CrossRef](#)]
10. Azevedo, C.; Sziogyarto, Z.; Saiardi, A. The signaling role of inositol hexakisphosphate kinases (IP6Ks). *Adv. Enzym. Regul.* **2011**, *51*, 74–82. [[CrossRef](#)] [[PubMed](#)]
11. Bhandari, R.; Chakraborty, A.; Snyder, S.H. Inositol Pyrophosphate Pyrotechnics. *Cell Metab.* **2007**, *5*, 321–323. [[CrossRef](#)] [[PubMed](#)]
12. Burton, A.; Hu, X.; Saiardi, A. Are inositol pyrophosphates signalling molecules? *J. Cell. Physiol.* **2009**, *220*, 8–15. [[CrossRef](#)]
13. Lin, H.; Fridy, P.C.; Ribeiro, A.A.; Choi, J.H.; Barma, D.K.; Vogel, G.; Falck, J.R.; Shears, S.B.; York, J.D.; Mayr, G.W. Structural analysis and detection of biological inositol pyrophosphates reveal that the family of VIP/diphosphoinositol pentakisphosphate kinases are 1/3-kinases. *J. Biol. Chem.* **2009**, *284*, 1863–1872. [[CrossRef](#)]
14. Majerus, P.W. A discrete signaling function for an inositol pyrophosphate. *Sci. STKE* **2007**, *2007*, pe72. [[PubMed](#)]
15. Mulugu, S.; Bai, W.; Fridy, P.; Bastidas, R.J.; Otto, J.C.; Dollins, D.E.; Haystead, T.A.; Ribeiro, A.A.; York, J.D. A Conserved Family of Enzymes That Phosphorylate Inositol Hexakisphosphate. *Science* **2007**, *316*, 106–109. [[CrossRef](#)] [[PubMed](#)]
16. Onnebo, S.M.N.; Saiardi, A. Inositol Pyrophosphates Get the Vip1 Treatment. *Cell* **2007**, *129*, 647–649. [[CrossRef](#)]
17. Wang, H.; Falck, J.R.; Hall, T.M.T.; Shears, S.B. Structural basis for an inositol pyrophosphate kinase surmounting phosphate crowding. *Nat. Chem. Biol.* **2011**, *8*, 111–116. [[CrossRef](#)] [[PubMed](#)]
18. Wundenberg, T.; Mayr, G.W. Synthesis and biological actions of diphosphoinositol phosphates (inositol pyrophosphates), regulators of cell homeostasis. *Biol. Chem.* **2012**, *393*, 979–998. [[CrossRef](#)]
19. Saiardi, A. Cell Signalling by Inositol Pyrophosphates. *Prokaryotic Cytoskelet.* **2012**, *59*, 413–443. [[CrossRef](#)]
20. Tusi, M.M.; York, J.D. Roles of inositol phosphates and inositol pyrophosphates in development, cell signaling and nuclear processes. *Adv. Enzyme Regul.* **2010**, *50*, 324–337.
21. Thota, S.G.; Bhandari, R. The emerging roles of inositol pyrophosphates in eukaryotic cell physiology. *J. Biosci.* **2015**, *40*, 593–605. [[CrossRef](#)]
22. Brown, N.W., Jr.; Marmelstein, A.M.; Fiedler, D. Chemical tools for interrogating inositol pyrophosphate structure and function. *Chem. Soc. Rev.* **2016**, *45*, 6311–6326. [[CrossRef](#)] [[PubMed](#)]
23. Lee, Y.-S.; Huang, K.; Quioco, F.A.; O’Shea, E.K. Molecular basis of cyclin-CDK-CKI regulation by reversible binding of an inositol pyrophosphate. *Nat. Chem. Biol.* **2008**, *4*, 25–32. [[CrossRef](#)] [[PubMed](#)]
24. Yin, M.-X.; Catimel, B.; Gregory, M.; Condron, M.; Kapp, E.; Holmes, A.B.; Burgess, A.W. Synthesis of an inositol hexakisphosphate (IP6) affinity probe to study the interactome from a colon cancer cell line. *Integr. Biol.* **2016**, *8*, 309–318. [[CrossRef](#)] [[PubMed](#)]
25. Lee, Y.-S.; Mulugu, S.; York, J.D.; O’Shea, E.K. Regulation of a Cyclin-CDK-CDK Inhibitor Complex by Inositol Pyrophosphates. *Science* **2007**, *316*, 109–112. [[CrossRef](#)]
26. Chakraborty, A.; Koldobskiy, M.A.; Bello, N.T.; Maxwell, M.; Potter, J.J.; Juluri, K.R.; Maag, D.; Kim, S.; Huang, A.S.; Dailey, M.J.; et al. Inositol pyrophosphates inhibit Akt signaling, thereby regulating insulin sensitivity and weight gain. *Cell* **2010**, *143*, 897–910. [[CrossRef](#)] [[PubMed](#)]
27. Luo, H.B.R.; Huang, Y.E.; Chen, J.M.C.; Saiardi, A.; Iijima, M.; Ye, K.Q.; Huang, Y.F.; Nagata, E.; Devreotes, P.; Snyder, S.H. Inositol pyrophosphates mediate chemotaxis in dictyostelium via pleckstrin homology domain-PtdIns(3,4,5)P3 interactions. *Cell* **2003**, *114*, 559. [[CrossRef](#)]
28. Albert, C.; Safrany, S.; Bembenek, E.M.; Reddy, K.M.; Falck, J.R.; Bröcker, M.; Shears, B.S.; Mayr, W.G. Biological variability in the structures of diphosphoinositol polyphosphates in *Dictyostelium discoideum* and mammalian cells. *Biochem. J.* **1997**, *327*, 553–560. [[CrossRef](#)]
29. Wu, M.; Dul, B.E.; Trevisan, A.J.; Fiedler, D. Synthesis and characterization of non-hydrolysable diphosphoinositol polyphosphate messengers. *Chem. Sci.* **2012**, *4*, 405–410. [[CrossRef](#)] [[PubMed](#)]
30. Zhang, H.; Thompson, J.; Prestwich, G.D. A Scalable Synthesis of the IP7 Isomer, 5-PP-Ins(1,2,3,4,6)P5. *Org. Lett.* **2009**, *11*, 1551–1554. [[CrossRef](#)]
31. Capolicchio, S.; Thakor, D.T.; Linden, A.; Jessen, H.J. Synthesis of Unsymmetric Diphospho-Inositol Polyphosphates. *Angew. Chem. Int. Ed.* **2013**, *52*, 6912–6916. [[CrossRef](#)]
32. Capolicchio, S.; Wang, H.; Thakor, D.T.; Shears, S.B.; Jessen, H.J. Synthesis of Densely Phosphorylated Bis-1,5-Diphospho-*myo*-Inositol Tetrakisphosphate and its Enantiomer by Bidirectional P-Anhydride Formation. *Angew. Chem. Int. Ed.* **2014**, *53*, 9508–9511. [[CrossRef](#)]

33. Pavlovic, I.; Thakor, D.T.; Bigler, L.; Wilson, M.; Laha, D.; Schaaf, G.; Saiardi, A.; Jessen, H.J. Prometabolites of 5-Diphospho-*myo*-inositol Pentakisphosphate. *Angew. Chem. Int. Ed.* **2015**, *54*, 9622–9626. [[CrossRef](#)]
34. Pavlovic, I.; Thakor, D.T.; Vargas, J.R.; McKinlay, C.J.; Hauke, S.; Anstaett, P.; Camuña, R.C.; Bigler, L.; Gasser, G.; Schultz, C.; et al. Cellular delivery and photochemical release of a caged inositol-pyrophosphate induces PH-domain translocation in cellulose. *Nat. Commun.* **2016**, *7*, 10622. [[CrossRef](#)]
35. Riley, A.M.; Wang, H.; Weaver, J.D.; Shears, S.B.; Potter, B.V.L. First synthetic analogues of diphosphoinositol polyphosphates: Interaction with PP-InsP5 kinase. *Chem. Commun.* **2012**, *48*, 11292–11294. [[CrossRef](#)]
36. Wu, M.; Chong, L.S.; Capolicchio, S.; Jessen, H.J.; Resnick, A.C.; Fiedler, D. Elucidating Diphosphoinositol Polyphosphate Function with Nonhydrolyzable Analogues. *Angew. Chem. Int. Ed.* **2014**, *53*, 7192–7197. [[CrossRef](#)] [[PubMed](#)]
37. Wu, M.; Chong, L.S.; Perlman, D.H.; Resnick, A.C.; Fiedler, D. Inositol polyphosphates intersect with signaling and metabolic networks via two distinct mechanisms. *Proc. Natl. Acad. Sci. USA* **2016**, *113*, E6757–E6765. [[CrossRef](#)] [[PubMed](#)]
38. Weaver, J.D.; Wang, H.; Shears, S.B. The kinetic properties of a human PPIP5K reveal that its kinase activities are protected against the consequences of a deteriorating cellular bioenergetic environment. *Biosci. Rep.* **2013**, *33*, e00022. [[CrossRef](#)] [[PubMed](#)]
39. Wang, H.; Godage, H.Y.; Riley, A.M.; Weaver, J.D.; Shears, S.B.; Potter, B.V.L. Synthetic Inositol Phosphate Analogs Reveal that PPIP5K2 Has a Surface-Mounted Substrate Capture Site that Is a Target for Drug Discovery. *Chem. Biol.* **2014**, *21*, 689–699. [[CrossRef](#)]
40. Shears, S.B.; Ali, N.; Craxton, A.; Bembenek, M.E. Synthesis and Metabolism of Bis-diphosphoinositol Tetrakisphosphate in Vitro and in Vivo. *J. Biol. Chem.* **1995**, *270*, 10489–10497. [[CrossRef](#)] [[PubMed](#)]
41. Craxton, A.; Caffrey, J.J.; Burkhart, W.; Safrany, S.; Shears, S.B. Molecular cloning and expression of a rat hepatic multiple inositol polyphosphate phosphatase. *Biochem. J.* **1997**, *328*, 75–81. [[CrossRef](#)]
42. Kilari, R.S.; Weaver, J.D.; Shears, S.B.; Safrany, S. Understanding inositol pyrophosphate metabolism and function: Kinetic characterization of the DIPP. *FEBS Lett.* **2013**, *587*, 3464–3670. [[CrossRef](#)] [[PubMed](#)]
43. Wundenberg, T.; Grabinski, N.; Lin, H.; Mayr, G.W. Discovery of InsP6-kinases as InsP6-dephosphorylating enzymes provides a new mechanism of cytosolic InsP6 degradation driven by the cellular ATP/ADP ratio. *Biochem. J.* **2014**, *462*, 173–184. [[CrossRef](#)] [[PubMed](#)]
44. Dollins, D.E.; Bai, W.; Fridy, P.C.; Otto, J.C.; Neubauer, J.L.; Gattis, S.G.; Mehta, K.P.M.; York, J.D. Vip1 is a kinase and pyrophosphatase switch that regulates inositol diphosphate signaling. *Proc. Natl. Acad. Sci. USA* **2020**, *117*, 9356–9364. [[CrossRef](#)] [[PubMed](#)]
45. Riley, A.M.; Trusselle, M.; Kuad, P.; Borkovec, M.; Cho, J.; Choi, J.H.; Qian, X.; Shears, S.B.; Spiess, B.; Potter, B.V.L. scyllo-Inositol Pentakisphosphate as an Analogue of *myo*-Inositol 1,3,4,5,6-Pentakisphosphate: Chemical Synthesis, Physicochemistry and Biological Applications. *ChemBioChem* **2006**, *7*, 1114–1122. [[CrossRef](#)]
46. Chung, S.-K.; Kwon, Y.-U.; Chang, Y.-T.; Sohn, K.-H.; Shin, J.-H.; Park, K.-H.; Hong, B.-J.; Chung, I.-H. Synthesis of all possible regioisomers of scyllo-Inositol phosphate. *Bioorganic Med. Chem.* **1999**, *7*, 2577–2589. [[CrossRef](#)]
47. Kwon, Y.-U.; Im, J.; Choi, G.; Kim, Y.-S.; Choi, K.Y.; Chung, S.-K. Synthesis of three enantiomeric pairs of scyllo-inositol phosphate and molecular interactions between all possible regioisomers of scyllo-inositol phosphate and inositol 1,4,5-trisphosphate 3-kinase. *Bioorganic Med. Chem. Lett.* **2003**, *13*, 2981–2984. [[CrossRef](#)]
48. Thomas, M.P.; Mills, S.J.; Potter, B.V.L. The “Other” inositols and their phosphates: Synthesis, biology, and medicine (with recent advances in *myo*-inositol chemistry). *Angew. Chem. Int.* **2016**, *55*, 1614–1650. [[CrossRef](#)]
49. Turner, B.L.; Cheesman, A.W.; Godage, H.Y.; Riley, A.M.; Potter, B.V.L. Determination of neo- and d-chiro-Inositol Hexakisphosphate in Soils by Solution 31P NMR Spectroscopy. *Environ. Sci. Technol.* **2012**, *46*, 4994–5002. [[CrossRef](#)]
50. Sureshan, K.M.; Kiyosawa, Y.; Han, F.; Hyodo, S.; Uno, Y.; Watanabe, Y. Resolution of synthetically useful *myo*-inositol derivatives using the chiral auxiliary O-acetylmandelic acid. *Tetrahedron Asymmetry* **2005**, *16*, 231–241. [[CrossRef](#)]
51. Babouri, R.; Traore, L.; Bekro, Y.-A.; Matveeva, V.I.; Sadykova, Y.M.; Voronina, J.K.; Burilov, A.R.; Ayad, T.; Volle, J.-N.; Virieux, D.; et al. Golden Face of Phosphine: Cascade Reaction to Bridgehead Methanophosphocines by Intramolecular Double Hydroarylation. *Org. Lett.* **2018**, *21*, 45–49. [[CrossRef](#)] [[PubMed](#)]
52. Losito, O.; Sziogyarto, Z.; Resnick, A.C.; Saiardi, A. Inositol Pyrophosphates and Their Unique Metabolic Complexity: Analysis by Gel Electrophoresis. *PLoS ONE* **2009**, *4*, e5580. [[CrossRef](#)]
53. Drašković, P.; Saiardi, A.; Bhandari, R.; Burton, A.; Ilc, G.; Kovačević, M.; Snyder, S.H.; Podobnik, M. Inositol Hexakisphosphate Kinase Products Contain Diphosphate and Triphosphate Groups. *Chem. Biol.* **2008**, *15*, 274–286. [[CrossRef](#)] [[PubMed](#)]
54. Wang, H.; Derose, E.F.; London, R.E.; Shears, S.B. IP6K Structure and the Molecular Determinants of Catalytic Specificity in an Inositol Phosphate Kinase Family. *Nat. Commun.* **2014**, *5*, 4178. [[CrossRef](#)]
55. The PyMOL Molecular Graphics System, version 2.0 Schrodinger, LLC. Available online: <https://pymol.org/2/support.html?#citing> (accessed on 9 June 2021).
56. Wormald, M.; Liao, G.; Kimos, M.; Barrow, J.; Wei, H. Development of a homogenous high-throughput assay for inositol hexakisphosphate kinase 1 activity. *PLoS ONE* **2017**, *12*, e0188852. [[CrossRef](#)] [[PubMed](#)]
57. Paudel, H.; Carlson, G. The ATPase activity of phosphorylase kinase is regulated in parallel with its protein kinase activity. *J. Biol. Chem.* **1991**, *266*, 16524–16529. [[CrossRef](#)]
58. Armstrong, R.N.; Kondo, H.; Kaiser, E.T. Cyclic AMP-dependent ATPase activity of bovine heart protein kinase. *Proc. Natl. Acad. Sci. USA* **1979**, *76*, 722–725. [[CrossRef](#)]

59. Ward, N.E.; O'Brian, C.A. The intrinsic ATPase activity of protein kinase C is catalyzed at the active site of the enzyme. *Biochemistry* **1992**, *31*, 5905–5911. [[CrossRef](#)]
60. Ahmad, S.; Hughes, M.A.; Johnson, G.L.; Scott, J.E. Development and Validation of a High-Throughput Intrinsic ATPase Activity Assay for the Discovery of MEKK2 Inhibitors. *J. Biomol. Screen.* **2013**, *18*, 388–399. [[CrossRef](#)] [[PubMed](#)]
61. Fox, T.; Fitzgibbon, M.J.; Fleming, M.A.; Hsiao, H.-M.; Brummel, C.L.; Su, M.S.-S. Kinetic mechanism and ATP-binding site reactivity of p38gamma MAP kinase. *FEBS Lett.* **1999**, *461*, 323–328. [[CrossRef](#)]
62. Ferreira-Cerca, S.; Sagar, V.; Schaefer, T.; Diop, M.; Wesseling, A.-M.; Lu, H.; Chai, E.; Hurt, E.; LaRonde-LeBlanc, N. ATPase-dependent role of the atypical kinase Rio2 on the evolving pre-40S ribosomal subunit. *Nat. Struct. Mol. Biol.* **2012**, *19*, 1316–1323. [[CrossRef](#)]
63. Trajtenberg, F.; Graña, M.; Ruétalo, N.; Botti, H.; Buschiazzo, A. Structural and Enzymatic Insights into the ATP Binding and Autophosphorylation Mechanism of a Sensor Histidine Kinase. *J. Biol. Chem.* **2010**, *285*, 24892–24903. [[CrossRef](#)] [[PubMed](#)]
64. Bruker. *SADABS (Version 2.05)*, *SMART (Version 5.631)*, *SAINTE (Version 6.45)* and *SHELXTL (Version 6.14)*; Bruker AXS Inc.: Madison, WI, USA, 2003.
65. Sheldrick, G.M. Crystal structure refinement with SHELXL. *Acta Cryst.* **2015**, *71*, 3–8.
66. Wang, X.J.; Xu, B.; Mullins, A.B.; Neiler, F.K.; Etkorn, F.A. Conformationally locked isostere of phosphoSer–cis-pro inhibits pin1 23-fold better than phosphoSer–trans-pro isostere. *J. Am. Chem. Soc.* **2004**, *126*, 15533–15542. [[CrossRef](#)]
67. Bhandari, R.; Saiardi, A.; Ahmadibeni, Y.; Snowman, A.M.; Resnick, A.C.; Kristiansen, T.Z.; Molina, H.; Pandey, A.; Werner, J.K.; Juluri, K.R.; et al. Protein pyrophosphorylation by inositol pyrophosphates is a posttranslational event. *Proc. Natl. Acad. Sci. USA* **2007**, *104*, 15305–15310. [[CrossRef](#)]
68. Saiardi, A.; Erdjument-Bromage, H.; Snowman, A.M.; Tempst, P.; Snyder, S.H. Synthesis of diphosphoinositolpentakisphosphate by a newly identified family of higher inositol polyphosphate kinases. *Curr. Biol.* **1999**, *9*, 1323–1326. [[CrossRef](#)]
69. Azevedo, C.; Saiardi, A. Extraction and analysis of soluble inositol polyphosphates from yeast. *Nat. Protoc.* **2006**, *1*, 2416–2422. [[CrossRef](#)] [[PubMed](#)]
70. Onnebo, S.M.N.; Saiardi, A. Inositol pyrophosphates modulate hydrogen peroxide signalling. *Biochem. J.* **2009**, *423*, 109–118. [[CrossRef](#)]
71. Jones, G.; Willett, P.; Glen, R.C.; Leach, A.R.; Taylor, R. Development and validation of a genetic algorithm for flexible docking. *J. Mol. Biol.* **1997**, *267*, 727–748. [[CrossRef](#)]
72. Dennington, R.; Keith, T.A.; Millam, J.M. *GaussView, Version 6.1*; Semichem Inc.: Shawnee Mission, KS, USA, 2016.
73. Avogadro: An Open-Source Molecular Builder and Visualization Tool. Version 1.2.0. Available online: <http://avogadro.cc/> (accessed on 11 June 2021).
74. Riley, A.M.; Unterlass, J.; Konieczny, V.; Taylor, C.W.; Helleday, T.; Potter, B.V.L. A synthetic diphosphoinositol phosphate analogue of inositol trisphosphate. *MedChemComm* **2018**, *9*, 1105–1113. [[CrossRef](#)]
75. Salentin, S.; Schreiber, S.; Haupt, V.J.; Adasme, M.F.; Schroeder, M. PLIP: Fully automated protein–ligand interaction profiler. *Nucleic Acids Res.* **2015**, *43*, W443–W447. [[CrossRef](#)] [[PubMed](#)]